Chemical Geology 454 (2017) 1–14

Contents lists available at ScienceDirect

Chemical Geology

journal homepage: www.elsevier.com/locate/chemgeo

Invited Research Article

Linear correlations in bamboo coral $\delta^{13}C$ and $\delta^{18}O$ sampled by SIMS and micromill: Evaluating paleoceanographic potential and biomineralization mechanisms using $\delta^{11}B$ and Δ_{47} composition

Casey Saenger [a,*], Rinat I. Gabitov [b], Jesse Farmer [c], James M. Watkins [d], Robert Stone [e]

[a] Joint Institute for the Study of the Atmosphere and Ocean, University of Washington, Seattle, WA, USA
[b] Department of Geosciences, Mississippi State University, Mississippi State, MS, USA
[c] Earth and Environmental Sciences and Lamont-Doherty Earth Observatory of Columbia University, New York, NY, USA
[d] Department of Geological Sciences, University of Oregon, Eugene, OR, USA
[e] Auke Bay Laboratories, Alaska Fisheries Science Center, NOAA Fisheries, Juneau, AK, USA

ARTICLE INFO

Article history:
Received 1 September 2016
Received in revised form 9 February 2017
Accepted 11 February 2017
Available online 16 February 2017

Keywords:
Deep sea corals
Paleoclimate
Oxygen isotope
Clumped isotope
Boron isotope
SIMS
Vital effect

ABSTRACT

Bamboo corals represent an intriguing paleoceanographic archive with the potential to reconstruct variations throughout the water column over multiple centuries. Realizing this potential partially depends on if, and at what resolution, timeseries of variability can be generated. Recent work demonstrates that bamboo coral growth temperature, averaged over its entire lifespan, can be derived from linear correlations in its carbon and oxygen isotope composition ($\delta^{13}C$, $\delta^{18}O$) when the apparent equilibrium fractionations for a coral's growth rate and calcifying pH are used. Building on this method, this study applies it to coeval coral skeleton to assess the possibility of extracting paleoceanographic timeseries from bamboo coral skeletons. Using boron isotope ($\delta^{11}B$) based pH estimates, micromilled samples yield accurate paleotemperatures with uncertainties of <2 °C, whose precision could be improved to <1 °C if additional sampling yielded more robust regressions. This provides strong evidence that decadal-scale temperature reconstructions may be extracted from bamboo corals. Complementary SIMS data generated at annual to inter-annual resolution often yield accurate temperatures, but with greater uncertainty that is always >2 °C. This is attributed to the inability to measure $\delta^{13}C$ and $\delta^{18}O$ in exactly the same skeleton, as is the case for micromilled samples. A micromilled sampling strategy is therefore likely the most practical means of applying the method. Carbonate clumped isotopes (Δ_{47}) estimate temperatures slightly warmer than observed, suggesting they may not accurately record the subtle variations of the latest Holocene. When interpreted in conjunction, $\delta^{18}O$, $\delta^{11}B$ and Δ_{47} data suggest that pH up-regulation plays a role in generating linear $\delta^{13}C$-$\delta^{18}O$ trends. However, oxygen isotope fractionation and Δ_{47} are lower than would be predicted by pH alone. Potential explanations for this discrepancy include biological processes that favor the incorporation of carbonate ion into coral skeleton, uncertainties in the $\delta^{11}B$-pH proxy, the influence of magnesium on calcite-fluid isotope fractionation, or uncertainties in the fractionation factors used to calculate apparent equilibrium. Despite some remaining uncertainties, the method can resolve many observed decadal-scale thermocline temperature anomalies, suggesting that appropriately located bamboo corals could help constrain the behavior of similar temporal variability prior to instrumental monitoring.

© 2017 Published by Elsevier B.V.

1. Introduction

Changes in the temperature and structure of subsurface water masses are an important component of inter-annual to multidecadal climate variability (Chen and Tung, 2014; Dewitte et al., 2012; McDonagh et al., 2005; Miller and Schneider, 2000; Ramesh and Murtugudde, 2013; Rao et al., 2002; Zhang, 2007) that are expected to be altered by anthropogenic climate change (Capotondi et al., 2012; Collins et al., 2010). However, modern observations are heavily biased toward the surface, contributing to model error in subsurface temperature and thermocline structure (Li et al., 2015; Thompson and Cheng, 2008; Xu et al., 2013). Deep sea corals are promising archives of past subsurface temperature variability that may extend the observational record due to their near global distribution, multidecadal to multicentennial lifespan and ability to be dated using radiometric techniques (Prouty et al., 2015; Robinson et al., 2014).

Among deep sea corals, "bamboo" coral genera (*Keratoisis* and *Isidella* sp.) are gorgonians that are common at depths of ~100–3500 m (Etnoyer and Morgan, 2005; Farmer et al., 2015a; Hill et al.,

* Corresponding author.
E-mail address: csaenger@uw.edu (C. Saenger).

http://dx.doi.org/10.1016/j.chemgeo.2017.02.014
0009-2541/© 2017 Published by Elsevier B.V.

2011; Kimball et al., 2014; Stone, 2014) where they precipitate high magnesium (Mg) calcite skeletons throughout multidecadal to century-long lifespans (Andrews et al., 2009; Farmer et al., 2015b; Sherwood and Edinger, 2009). Inferred calcification at near ambient pH (Farmer et al., 2015a) leads to modest radial growth rates of ~12–160 μm/yr (Andrews et al., 2009; Farmer et al., 2015b; Thresher et al., 2009). This is sufficiently fast to potentially yield annual to decadal-scale paleoenvironmental reconstructions that reach into the preindustrial era, and bamboo corals have been explored as proxies for numerous marine variables (Farmer et al., 2015a; Hill et al., 2012, 2014b; LaVigne et al., 2011) including temperature (Hill et al., 2011; Kimball et al., 2014; Thresher et al., 2004, 2010).

Reconstructing temperature in bamboo corals using traditional paleothermometers, such as the oxygen isotope composition of calcite (McCrea, 1950; O'Neil et al., 1969), has been complicated by clear evidence for biologically-mediated and/or kinetic effects on the oxygen isotope composition ($\delta^{18}O$) of bamboo coral skeleton (Hill et al., 2011; Kimball et al., 2014; Thresher and Neil, 2016). However, non-equilibrium $\delta^{18}O$ values are typically accompanied by proportional deviations in their carbon isotope composition ($\delta^{13}C$), which produce strong linear correlations between the two. Smith et al. (2000) proposed a method to exploit these $\delta^{18}O$-$\delta^{13}C$ trends to estimate the growth temperature of aragonitic deep sea corals. Specifically, trends were extrapolated to the point where coral $\delta^{13}C$ equaled that of the surrounding dissolved inorganic carbon (DIC) (i.e. $\delta^{13}C_{coral}$-$\delta^{13}C_{DIC} = 0‰$), and the complementary $\delta^{18}O_{coral}$-$\delta^{18}O_{water}$ at that point was assumed to reflect apparent equilibrium fractionation (Grossman and Ku, 1986). Assuming a constant $\delta^{18}O_{water}$, the mean growth temperature over a coral's lifespan could be calculated. Application of this empirical 'lines method' to calcitic bamboo corals suggested that the approach could yield reasonable estimates of mean growth temperature, but systematic offsets from abiogenic experiments indicated that kinetic and/or vital effects had not been completely accounted for (Hill et al., 2011; Kimball et al., 2014). Recent work indicates that this offset can largely be resolved by using model II regressions and apparent equilibrium isotope fractionation factors that are appropriate for the rate and pH of bamboo coral growth (Saenger and Watkins, 2016).

Despite considerable progress, the $\delta^{18}O$-$\delta^{13}C$ trends used in the studies above were collected in skeleton deposited throughout each coral's lifespan, and therefore were limited to single temperature estimates that averaged multiple decades or centuries. Such long-term averages cannot characterize the decadal-scale trends that are relevant for understanding the climatic significance of subsurface temperature variability. Intriguingly however, both Hill et al. (2011) and Kimball et al. (2014) found that linear $\delta^{18}O$-$\delta^{13}C$ trends could occur in a single skeletal band of approximately the same age, which raises the possibility that fine sampling of concentric bamboo coral growth rings could yield timeseries of paleotemperature variability. At an optimistic micromilled sampling resolution of ~150 μm, typical bamboo coral growth rates suggest that such timeseries could achieve inter-annual to decadal resolution. In contrast, secondary ionization mass spectrometry (SIMS) can measure coral $\delta^{18}O$ and $\delta^{13}C$ at spatial resolutions of tens of microns (Blamart et al., 2005; Rollion-Bard et al., 2003a), which may allow for paleotemperature timeseries with annual or better temporal resolution.

The accurate interpretation of potential bamboo coral-based paleotemperature timeseries would benefit from a better understanding of mechanism(s) responsible for $\delta^{18}O$-$\delta^{13}C$ trends. Although not exhaustive (e.g. Rollion-Bard et al., 2003b; Rollion-Bard et al., 2010) two biologically mediated mechanisms that may explain bamboo coral $\delta^{18}O$-$\delta^{13}C$ correlations are carbon and oxygen isotopic changes at the site of calcification from 1) the sluggish isotopic equilibration of calcifying fluid DIC species relative to rapid coral calcification (McConnaughey, 1989; Smith et al., 2000), hereafter referred to as the 'McConnaughey' mechanism and 2) pH-induced shifts in DIC speciation and the flux of metabolic carbon to the calcifying fluid (Adkins et al., 2003), hereafter referred to as the 'Adkins' mechanism. Rollion-Bard et al.'s (2003b) model combined these concepts to develop a model that depended both on pH and the residence time of calcifying fluid. Although these models were developed using data from aragonitic scleractinian corals, it is not unreasonable that their fundamental principles could operate in other marine calcifyers such as high-Mg calcite bamboo corals. However, an obvious complication to determining the relevance of these mechanisms to bamboo corals is that they are both capable of producing similar $\delta^{18}O$-$\delta^{13}C$ trends.

The clumped isotope composition (Δ_{47}) of carbonates reflects their abundance of ^{18}O—^{13}C bonds, which can vary with temperature (Eiler, 2007), but is also sensitive to kinetic effects, pH and other variables (Affek et al., 2008; Kluge et al., 2014; Tripati et al., 2015). No resolvable dependence of Δ_{47} on mineralogy has been measured between calcite and aragonite (Defliese et al., 2015) suggesting that it is appropriate to compare abiogenic calcite experiments to high-Mg calcite bamboo corals. The additional information provided by Δ_{47} data may therefore help evaluate the degree to which the McConnaughey and/or Adkins mechanisms contribute to linear $\delta^{18}O$-$\delta^{13}C$ trends in bamboo corals. For example, both a non-equilibrium DIC pool and high calcifying fluid pH potentially affect coral Δ_{47} (Saenger et al., 2012; Thiagarajan et al., 2011; Tripati et al., 2015), but in opposite directions providing a unique signature in $\delta^{18}O$ versus Δ_{47} space. This approach has been used to suggest that the slow hydration and/or hydroxylation of metabolic CO_2 contributes to higher than expected Δ_{47}, and cooler than observed temperature, in some aragonitic deep sea corals (Spooner et al., 2016).

This study has two primary goals. First, we will determine if meaningful paleotemperature timeseries can be extracted from $\delta^{18}O$-$\delta^{13}C$ trends in coeval portions of bamboo coral internodes. Second, we will evaluate if the McConnaughey and/or Adkins models are consistent with what little is known about bamboo coral biomineralization. The first goal will be achieved by applying the methods developed by Saenger and Watkins, 2016 to bamboo coral $\delta^{18}O$ and $\delta^{13}C$ along sampling transects of approximately constant age from both high spatial resolution SIMS analyses and coarser micromilled samples measured via isotope ratio mass spectrometry (IRMS). The second goal will be accomplished by evaluating if bamboo coral Δ_{47} is consistent with the Δ_{47}-$\delta^{18}O$ trends expected for each physicochemical model.

2. Materials and methods

2.1. Sample sites

The two bamboo corals analyzed in this study were collected via longline survey from the Gulf of Alaska (Fig. 1; Table 1). *Isidella tentaculum* specimen AB13-0005 (58.178 N, 138.982 W) was collected in July 2008 from a depth of 701 m, while *Keratoisis* sp. specimen AB12-0156 (57.882 N, 137.435 W) was recovered in July 2006 from a depth of 746 m. The specific methods of sample collection and identification are described in Andrews et al. (2009). That study calculated bamboo coral radial growth rates via ^{210}Pb analyses, and found rates

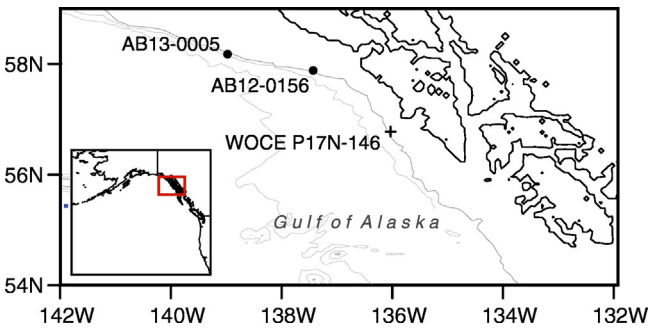

Fig. 1. Locations of bamboo coral collection and WOCE station P17N-146 used to estimate some environmental variables.

Table 1
Inferred conditions at bamboo coral sampling sites.

ID	Taxon	Lat	Lon	Depth (m)	$\delta^{18}O_w$ (‰ SMOW)[a]	$\delta^{13}C_{DIC}$ (‰ PDB)[b]	T (°C)	T error (°C)	Salinity (psu)	Salinity error (psu)	LogR (mol/m^2/s)[c]	LogR error (mol/m^2/s)[c]	pH_{sw}	pH error	DIC (umol/kg)	DIC error (umol/kg)
AB13-0005	*Isidella tentaculum*	58.18	−138.98	701	−0.16	−0.67	3.67	0.76	34.19	0.12	−7.3	0.1	7.54	0.07	2343	28
AB12-0156	*Keratoisis* sp.	57.88	−137.44	746	−0.16	−0.67	3.78	0.67	34.21	0.11	−7.1	0.1	7.54	0.07	2346	24

[a] From Legrande and Schmidt (2006).
[b] From WOCE station P17N-146.
[c] From Andrews et al. (2009). AB13-0005 assumes growth rate of similar Gulf of Alaska *Isidella tentaculum* coral.

of 0.056 ± 0.019 and 0.100 ± 0.020 mm yr^{-1}, respectively, for AB12-0156 and an *Isidella tentaculum* specimen similar to AB13-0005. This is equivalent to log $R = -7.3 \pm 0.1$ and -7.1 ± 0.1 mol/m^2/s, respectively (assuming a calcite density of 2.71 g/cm^3).

Mean annual temperature at the AB13-0005 site is estimated to be 3.67 ± 0.76 °C, while that of AB12-0156 is 3.78 ± 0.67 °C (Locarnini et al., 2010). Conservative estimates of the salinity, DIC and alkalinity at each site derived from the ranges in Fisheries and Oceans Canada Line P data (Table 1). These data estimate pH (total) was 7.54 ± 0.07 for both sites. The $\delta^{18}O_{water}$ at each site was estimated to be −0.16‰ (VSMOW) from the closest grid point in the gridded product of LeGrande and Schmidt (2006). LeGrande and Schmidt (2006) do not provide error estimates for these values, but the RMS error for North Pacific intermediate waters is reported to be 0.081‰. The $\delta^{13}C_{DIC}$ for both sites is estimated to be −0.67 ± 0.1‰ based on the 708–811 m average at WOCE station P17N-146 (56.778 N, 136.037 W; Fig. 1).

2.2. Sample preparation and analysis

Cylindrical cross-sections ~7–10 mm in height were cut from the basal internode of each specimen using a low-speed, Buehler IsoMet saw (Fig. 2a). Each subsample was then cut in half again, with the facing side of the lower half reserved for IRMS analyses and the complementary portion of the upper face used for SIMS (Fig. 2b). This approach allowed IRMS and SIMS analyses on nearly identical skeletal regions. Neither coral specimen showed evidence for bioerosion or diagenesis, consistent with previous evidence for good preservation in bamboo corals (Noé and Dullo, 2006).

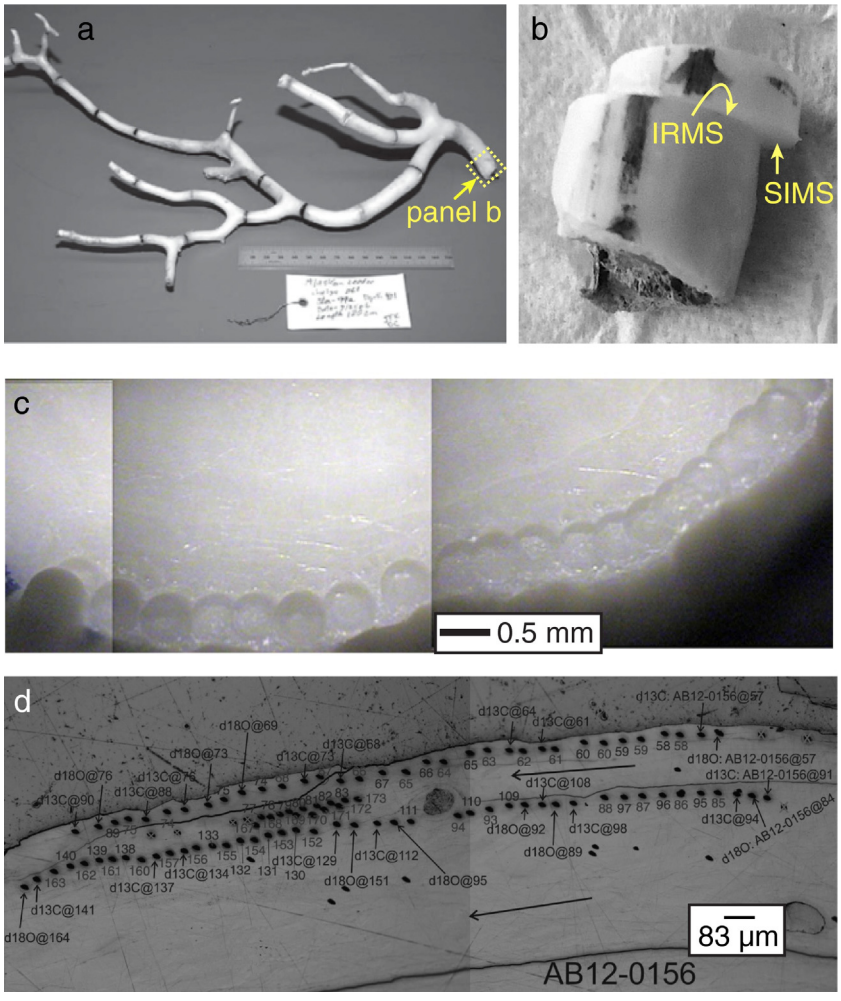

Fig. 2. Bamboo coral sampling strategy in which a) a segment is cut from the basal internode b) bisected so that facing surfaces can be sampled via c) micromill or d) SIMS.

Powders for IRMS-based $\delta^{18}O$ and $\delta^{13}C$ analyses were drilled in a transect of approximately the same age that paralleled the outer margin of each coral (Fig. 2c) using a Merchantek/New Wave MicroMill. Each sample integrated skeleton in a circular region ~250 μm in diameter and ~300 μm deep that yielded ~40 μg of powder. The entire transect was then resampled to a depth of ~7 mm to produce ~35 mg of powder required for replicate Δ_{47} measurements and ~2 mg of powder for boron isotope ($\delta^{11}B$) estimates of coral calcifying fluid pH.

2.3. IRMS $\delta^{18}O$, $\delta^{13}C$ and Δ_{47}

IRMS-based $\delta^{18}O$ and $\delta^{13}C$ analyses as well as Δ_{47} measurements were made at the University of Washington's IsoLab using previously described procedures (Peters et al., 2013; Tobin et al., 2011; Kelson et al., 2017). Briefly, for $\delta^{18}O$ and $\delta^{13}C$ analyses, ~40 μg of calcite powder was measured using a Kiel III Carbonate Device attached to a Delta Plus IRMS (Thermo Scientific). Samples were reacted at 70 °C and are reported in VPDB using marble and calcite internal standards that have been calibrated against NBS18, NBS19 and LSVEC. Long-term precision (1 s.d.) for this instrument is 0.10‰ and 0.07‰ for $\delta^{18}O$ and $\delta^{13}C$, respectively. For Δ_{47} analyses, 6–8 mg of powder was reacted in a common acid bath at 90 °C and cryogenically purified using an automated system. Purified CO_2 was analyzed using a multi-collector MAT253 IRMS (Thermo Scientific) configured to measure masses 44–49 inclusive. Reference gas piped into this instrument eliminated the need for reference gas refilling, and ensured sample and standard are balanced throughout a run. The correction for ^{17}O interference used a value of 0.528 to relate abundances of ^{17}O and ^{18}O (Brand et al., 2010), which has been shown to increase the accuracy of Δ_{47} and eliminate discrepancies among abiogenic Δ_{47}-temperature calibrations (Schauer et al., 2016). Pressure baseline correction (He et al., 2012) was made by measuring the reference gas signal 0.0084 V down voltage of the mass 46 peak center. Samples were converted to the absolute Δ_{47} reference frame (Dennis et al., 2011) using a suite of CO_2 samples equilibrated with deionized and isotopically enriched water at 4, 60 and 1000 °C. All Δ_{47} values reflect 90 °C acid digestions without the application of an acid fractionation factor to approximate a 25 °C reaction. Long-term Δ_{47} precision based on repeat measurements of an in-house calcite standard is 0.018‰ (1 s.d.).

2.4. SIMS $\delta^{18}O$ and $\delta^{13}C$

The complementary half of each coral subsample was mounted in epoxy (EpoxiCure, Buehler) such that the surface exposed for SIMS analysis was effectively identical to micromilled transect. The mount was polished with 400, 600, 800, and 1200 grit SIC paper (Buehler) and 1 μm alumina powder following ultrasonication in deionized water. The $\delta^{13}C$ and $\delta^{18}O$ along transects following the edge of each coral were measured in separate sessions using a CAMECA ims 1270 ion microprobe at UCLA. Unlike IRMS, SIMS cannot measure $\delta^{13}C$ and $\delta^{18}O$ simultaneously, so that samples were alternated along each transect (Figs. 2d, 3, 4). In addition to the most recent growth layer (i.e. T1), two concentric transects of older growth were sampled approximately parallel to the outer edge in AB12-0156 (T2 and T3; Fig. 3).

For $\delta^{13}C$ measurements, polished coral sections were analyzed using a 4.7–5.5 nA Cs^+ primary beam with a lateral dimension of 20–25 μm. Negative secondary ions ^{12}C and ^{13}C were simultaneously measured by Faraday Cup (FC, L2′) and electron multiplier (EM, axial) using multi-collection set-up for a mass resolving power (MRP = M/ΔM) of 5500, which is sufficient for resolving interferences with the ^{12}C and ^{13}C peaks (Rollion-Bard et al., 2003a). FC background and EM dead time corrections were performed for each measurement. Raw intensity of the minor isotope varied from 2.3×10^5 to 2.9×10^5 counts per second (cps). Before data collection the sample surface was sputtered for 10 s with automatic beam centering in field aperture. Both masses were measured for 15 cycles with a duration of 10 s per cycle. Ten spot analyses of calcium carbonate reference materials (MEX and NBS-19 calcites) yielded a precision of 0.4–0.5‰ (1 s.d.). The MEX standard was analyzed routinely after every 5–8 measurements of the coral calcite.

Oxygen isotope analyses were conducted during the two days following $\delta^{13}C$ measurements using a method similar to that of Gabitov et al. (2012). Briefly, a 4.0–4.8 nA Cs^+ primary beam with a lateral dimension of 20–25 μm at the sample surface was employed to measure

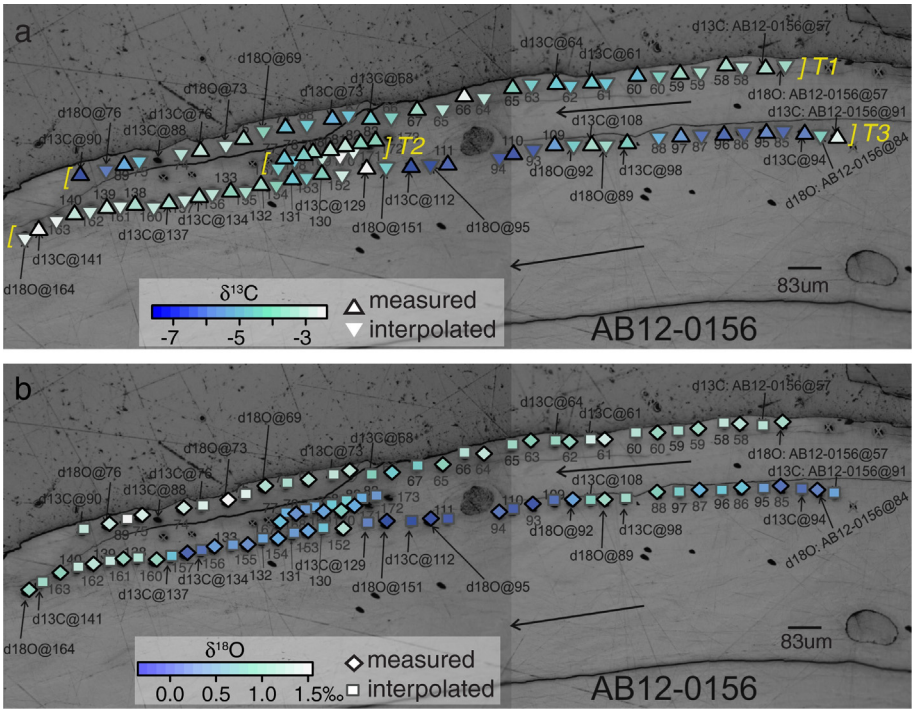

Fig. 3. Sample locations and stable isotope results for AB12-0156. T1, T2 and T3 refer to sampling tracks 1, 2 and 3. Interpolated values (inverted triangles, squares) fall between measured values.

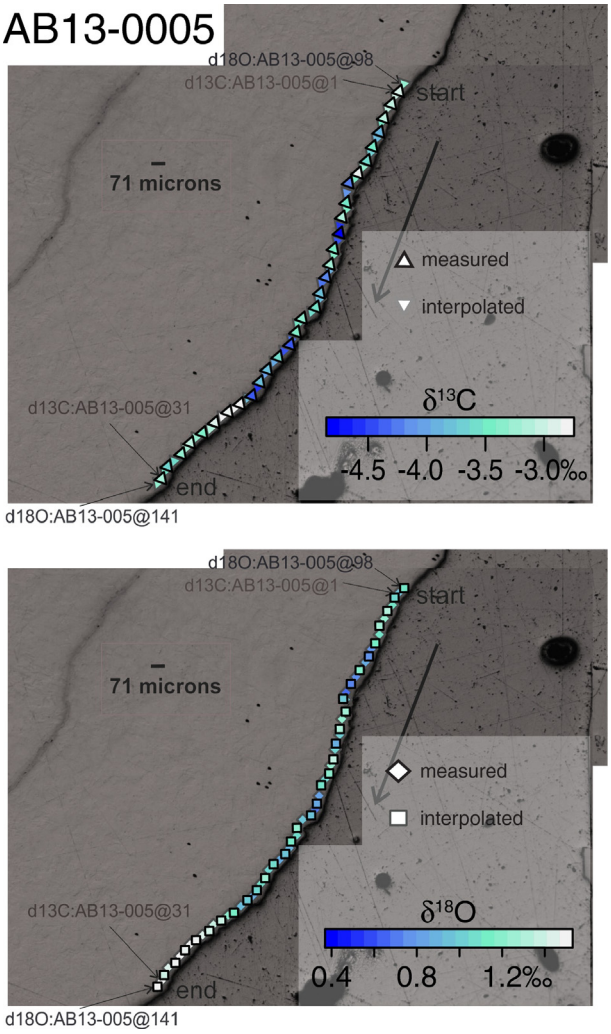

Fig. 4. As in Fig. 3 for AB13-0005.

^{16}O and ^{18}O simultaneously by FC using multi-collection detectors L′2 and H′2. The MRP was 2000, which is sufficient for resolving hydride interference with the ^{18}O peak (Fayek et al., 2002). The raw intensity of the minor isotope varied from 6.8×10^6 to 8.1×10^6 cps. The total sputtering time prior to acquisition was 120 s, which was sufficient to reach a steady $^{18}O/^{16}O$ value over the 12 cycles of the analysis on a single spot. Ten spot analyses of NBS19 yielded a precision of 0.2–0.3‰ (1 s.d.). The standard was analyzed routinely after every 5–8 measurements of the coral sample.

Because SIMS oxygen and carbon isotope data do not derive from identical locations, the $\delta^{13}C$ at the site of $\delta^{18}O$ spots, and vice versa, was calculated using ordinary kriging with the necessary covariance parameters estimated from a weighted least squares exponential fit of sample variograms. Furthermore, a constant correction was applied to SIMS-based $\delta^{13}C$ and $\delta^{18}O$ so that the mean for each coral was identical to the corresponding milled mean. This correction was −0.947‰ and +2.959‰ for AB13-0005 $\delta^{13}C$ and $\delta^{18}O$, respectively, and −1.417‰ and +2.076‰ for AB12-0156 $\delta^{13}C$ and $\delta^{18}O$, respectively (see online Supplementary material). Although the Mg content of carbonates is known to affect SIMS $\delta^{18}O$ with a sensitivity of about −0.3‰ per weight percent MgO (Rollion-Bard and Marin-Carbonne, 2011), the ~3 wt% MgO in bamboo corals (Thresher et al., 2007, 2010) could only account for ~1‰ of this offset. Furthermore, it is important to note that these corrections only change absolute values, not variations between data points, and therefore would only influence regression intercepts, not slopes.

2.5. $\delta^{11}B$

Boron isotopes were measured at the Lamont-Doherty Earth Observatory using established negative thermal ionization mass spectrometry (TIMS) procedures (Hemming and Hanson, 1994) and the detailed methodology of Farmer et al. (2015a). Briefly, 1.5 mg of homogenized coral powder was cleaned of organic matter with 1% ultrapure H_2O_2 buffered in 0.1 M NaOH, then rinsed with boron-free MQ water (>18.2 MΩ). Cleaned powders dissolved in 2 N HCl and loaded onto zone-refined Re filaments with 1 μL of a boron-free seawater solution. Boron isotope ratios were measured as $^{10}BO_2^-$ and $^{11}BO_2^-$ on a Thermo Triton multicollector TIMS and are expressed in delta notation relative to the NIST 951 boric acid standard reference material. An estimate of the pH at which each coral calcified was then calculated from their $\delta^{11}B$, the $\delta^{11}B$ of seawater (39.61‰; Foster et al., 2010), the aqueous boron fraction factor at 25 °C (1.0272, Klochko et al., 2006) and the boron system equilibrium constant (pK_B) at their temperature, salinity and depth (Dickson, 1990) (see Farmer et al., 2015a, equation 3). We calculate a pK_B of 8.8243 and 8.8228 for AB13-0005 and AB12-0156, respectively.

2.6. Estimates of apparent equilibrium

True equilibrium carbon and oxygen isotope fractionation (e.g. Coplen, 2007) is unlikely to be achieved at the growth rates of either laboratory experiments or biogenic carbonates (log $R \approx -8$ to -5.0 mol/m^2/s) (Watkins et al., 2013, 2014). In light of this, we use the phrase 'apparent equilibrium' to describe the isotopic signature of abiogenic experiments precipitated at a given temperature, precipitation rate and pH (Dietzel et al., 2009; Gabitov et al., 2012; Kim and O'Neil, 1997; Watkins et al., 2014). As described by Saenger and Watkins, 2016, the apparent equilibrium carbon and oxygen isotope fractionation predicted by an ion-by-ion calcite growth model (Watkins and Hunt, 2015) at each bamboo coral's observed growth temperature, pH and growth rate is used to describe the isotope signature that would be expected in the absence of vital effects. Calcification pH and growth rate are constrained by $\delta^{11}B$ and ^{210}Pb, respectively. We express carbon isotope fractionation relative to DIC using $\Delta^{13}C$ as shorthand for $1000\ln\alpha_{calcite\text{-}DIC}$ and $\Delta^{18}O$ as shorthand for $1000\ln\alpha_{calcite\text{-}water}$.

Following Saenger and Watkins, 2016, model II linear regressions of $\Delta^{13}C$-$\Delta^{18}O$ data are first extrapolated to the apparent equilibrium $\Delta^{13}C$ ($\Delta^{13}C_{aeq}$) predicted by the Watkins and Hunt (2015) model at each coral's growth temperature, pH and rate. The complementary $\Delta^{18}O$ value at this point is assumed to reflect apparent equilibrium ($\Delta^{18}O_{aeq}$), from which temperature can be estimated using an independent abiogenic relationship (Watkins and Hunt, 2015; Saenger and Watkins, 2016). Consistent with the findings of Saenger and Watkins, 2016, and in the absence of the requisite coral and DIC radiocarbon data, we assume no ^{13}C depleted respired CO_2 is incorporated into either coral skeleton.

Uncertainties in $\Delta^{13}C_{aeq}$ arise primarily from imperfect $\Delta^{18}O$-$\Delta^{13}C$ trends, although errors in estimated pH and growth rate will also propagate to $\Delta^{18}O_{aeq}$, and ultimately calculated temperature. To account for this, $\Delta^{13}C_{aeq}$ was calculated for all pH and growth rates within these uncertainty bounds, and maximum and minimum values were used. The upper bound on $\Delta^{18}O_{aeq}$ was set by the upper 95% regression confidence interval for the linear trend extrapolated to the most positive $\Delta^{13}C_{aeq}$. Equivalently, the lower $\Delta^{18}O_{aeq}$ bound was set by the lower 95% confidence interval of trends extrapolated to the most negative $\Delta^{13}C_{aeq}$. The resulting range of $\Delta^{18}O_{aeq}$ estimates was then sampled 10,000 times to generate a distribution of temperature estimates (see Saenger and Watkins, 2016). The uncertainty in observed temperature was also sampled 10,000 times and used to calculate the root mean squared error (RMSE) of predicted temperature (Table 2).

Table 2
Regression correlation coefficients (r), *p*-values (p), count (n), slopes (m), intercepts (b), apparent equilibrium bounds, and root mean square temperature error (RMSE).

ID	r	p	n	m	m 2.5% ci	m 97.5% ci	b	b 2.5% ci	b 97.5% ci	$\Delta^{13}C_{aeq\ min}$ (‰)	$\Delta^{13}C_{aeq\ max}$ (‰)	$\Delta^{18}O_{aeq\ mean}$ (‰)	$\Delta^{18}O_{aeq\ s.d}$ (‰)	RMSE (°C)
AB12-0156 milled	0.95	1.1E−04	9	0.35	0.27	0.47	32.71	32.38	33.14	2.16	2.52	33.53	0.34	1.54
AB13-0005 milled	0.89	1.7E−06	17	0.40	0.31	0.52	32.93	32.67	33.26	2.09	2.48	33.85	0.30	1.94
AB12-0156 SIMS T1	0.01	9.5E−01	33	0.22	0.15	0.32	32.54	32.30	32.89	–	–	–	–	–
AB12-0156 SIMS T2	0.57	5.4E−02	12	0.22	0.13	0.39	31.90	31.59	32.43	2.16	2.52	32.42	0.38	5.25
AB12-0156 SIMS T3	0.56	8.9E−05	44	0.32	0.25	0.41	32.40	32.12	32.75	2.16	2.52	33.14	0.28	2.18
AB13-0005 SIMS	0.32	9.6E−03	63	0.49	0.38	0.62	33.17	32.87	33.55	2.09	2.48	34.28	0.35	3.56

2.7. Incorporation of Δ_{47} into previously proposed mechanisms

To evaluate if either the McConnaughey or Adkins mechanisms may be relevant to bamboo corals, we adapt each model for clumped isotope variability, and present data in $\Delta^{18}O$ versus Δ_{47} space. The master variable of the Adkins mechanism is pH. At a given temperature and salinity, biologically mediated up-regulation of calcifying fluid pH will shift the speciation of DIC toward carbonate ion (Fig. 5). The oxygen isotope fractionation factor for CO_3^{2-}-H_2O is smaller than HCO_3^--H_2O (Beck et al., 2005; Kim et al., 2014; Tripati et al., 2015; Usdowski et al., 1991; Wang et al., 2013), leading to lower $\Delta^{18}O$ values at higher pH. Similarly, the Δ_{47} of CO_3^{2-} is lower than HCO_3^- (Hill et al., 2014a; Tripati et al., 2015), implying that Δ_{47} will also decrease with biologically-mediated up-regulation. Therefore, the Adkins mechanism would be supported if coral $\Delta^{18}O$ and Δ_{47} values were both lower than abiogenic experiments precipitated at near neutral pH (e.g. Kelson et al., 2017) and fell along a line connecting HCO_3^- and CO_3^{2-}. To be consistent with Watkins and Hunt (2015), our calculations use the values of Wang et al. (2013) and Hill et al. (2014a), respectively, when calculating the $\Delta^{18}O$ and Δ_{47} of HCO_3^- and CO_3^{2-}. Other choices (e.g. Beck et al., 2005; Tripati et al., 2015) are also reasonable, but do not fundamentally change our results.

The McConnaughey model follows his original formulation (McConnaughey, 1989, 2003) in which the master variables are 1) the fraction of DIC used for calcification that derives from respired CO_2 as opposed to seawater, and 2) the time available for hydration and/or hydroxylation of that CO_2 prior to skeletogenesis. When little time is available for CO_2 to undergo hydration or hydroxylation, coral $\Delta^{18}O$ will be lower than the equilibrium value with a $\Delta^{18}O$ minimum that is set by the fraction of DIC derived from respired CO_2. Because CO_2 is the only molecule participating in hydration or hydroxylation capable of having multiply substituted isotopologues, we suggest that unequilibrated DIC in the McConnaughey model would inherit the Δ_{47} of aqueous CO_2. We estimate this value to be 0.31‰ higher than the Δ_{47} value of bicarbonate (Hill et al., 2014a; Tripati et al., 2015). Thus, the McConnaughey mechanism is supported when $\Delta^{18}O$ is lower, but Δ_{47} is higher, than the value predicted by abiogenic experiments precipitated at near neutral pH as previously suggested (Saenger et al., 2012; Spooner et al., 2016; Tripati et al., 2015). Consistent with evidence that little or no respired CO_2 is incorporated into bamboo coral skeleton (Farmer et al., 2015b; Roark et al., 2005), we model the McConnaughey mechanism using a respired CO_2 contribution of 4% (Saenger and Watkins, 2016) without allowing any time for equilibration, noting that this will be an upper bound on its effect. The calculations presented use the aqueous CO_2-H_2O and OH^--H_2O oxygen isotope fractionation factors of Wang et al. (2013), but we note that other reasonable choices (e.g. Usdowski and Hoefs, 1993) do not fundamentally change our results.

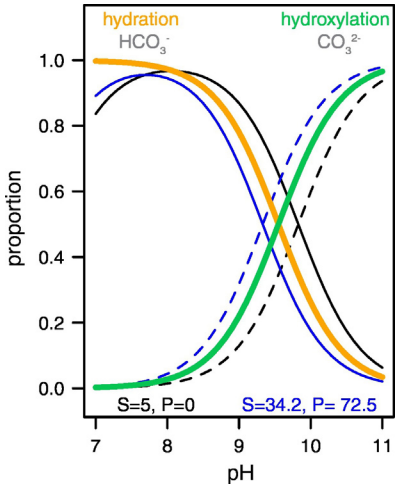

Fig. 5. Change in the proportion of HCO_3^- (solid lines) and CO_3^{2-} (dashed lines) in DIC with varying pH approximated for abiogenic experiments at 25 °C (black) and for the marine 3.7 °C growth environment of our bamboo corals (blue). S is salinity, P is pressure in bars. Also shown is the pH-dependent variation in the proportion of CO_2 expected to be converted to HCO_3^- via hydration (orange line) and hydroxylation (green line) at the temperature, salinity and depth of bamboo coral sites. (For interpretation of the references to colour in this figure legend, the reader is referred to the web version of this article.)

3. Results

3.1. Milled sampled

Milled stable carbon and oxygen isotope data and regression statistics are summarized in Table 2 and in the online Supplementary material. Briefly, $\delta^{18}O$ and $\delta^{13}C$ in coral AB13-0005 ranged from 1.00 to 1.28 ± 0.10‰ and −3.27 to −4.00 ± 0.07‰, respectively. Equivalent $\delta^{18}O$ and $\delta^{13}C$ ranges for AB12-0156 were 0.67 to 0.96 ± 0.10‰ ‰ and −3.93 to −4.76 ± 0.07‰, respectively. Taken at face value, these $\delta^{18}O$ values would predict temperatures of 8.0 to 9.2 °C for AB13-0005 and 9.4 to 10.7 °C for AB12-0156, using the $\delta^{18}O_{water}$ in Table 1 and the relationship of Kim and O'Neil (1997). Both corals exhibited robust $\Delta^{13}C$ versus $\Delta^{18}O$ model II regressions ($r = 0.89$ to 0.95, $p \ll 0.001$) with slightly steeper slopes than would be predicted by ordinary least squares (Fig. 6a,c).

3.2. SIMS data

SIMS-based $\delta^{18}O$ and $\delta^{13}C$ data varied over a wider range than milled data, and all sampling tracks exhibited a general positive correlation between $\Delta^{13}C$ and $\Delta^{18}O$ (Figs. 3, 4, 7, 8). AB13-0005 $\delta^{18}O$ and $\delta^{13}C$ varied from 0.74 to 1.49 ± 0.2‰ and −4.78 to −2.81 ± 0.4‰ for $\delta^{18}O$ and $\delta^{13}C$, respectively. Equivalent ranges in AB12-0156 were −0.30 to 1.53 ± 0.2‰ and −7.41 to −2.50 ± 0.4‰ for $\delta^{18}O$ and $\delta^{13}C$, respectively. Error estimates are based on repeat measurements of MEX and NBS-19 standards, and do not consider uncertainty in the value used to normalize SIMS data to milled data (Section 2.4). Interpreted solely in

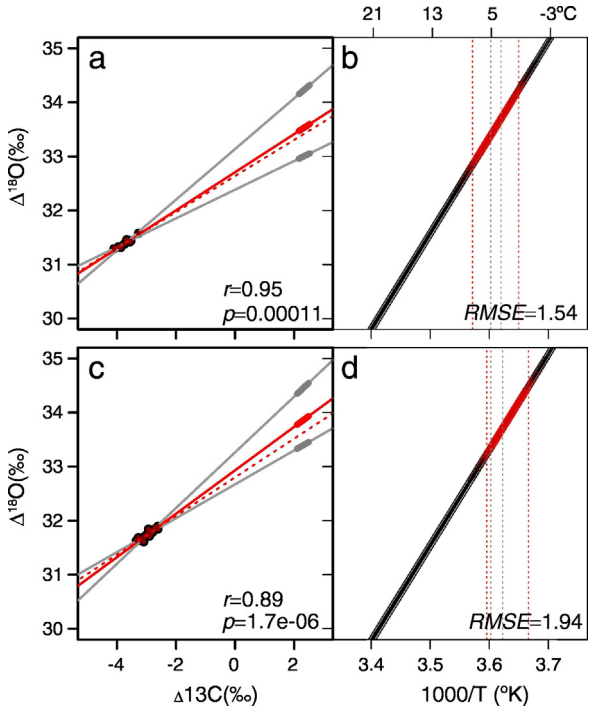

Fig. 6. Milled $\Delta^{13}C$ vs $\Delta^{18}O$ regressions for a) AB12-0156 and c) AB13-0005 showing best model II fit (red solid line) and its 95% confidence intervals (grey lines). Bold segments identify the range of $\Delta^{13}C_{aeq}$ values predicted by the Watkins and Hunt (2015) model for measured uncertainties in bamboo coral growth rate and pH. The shallower sloped model I regression is shown for reference (red dashed line). b) The abiogenic $\Delta^{18}O$-temperature relationships predicted for the range of AB12-0156 calcification pH and growth rate (solid black lines). Red shading reflects the range of $\Delta^{18}O_{aeq}$ and temperature selected in Monte Carlo iterations (see Section 2.6). Predicted temperature (vertical red dashed lines) are compared with observed temperature (vertical grey dashed lines) for reference. d) as in b) for AB13-0005. (For interpretation of the references to colour in this figure legend, the reader is referred to the web version of this article.)

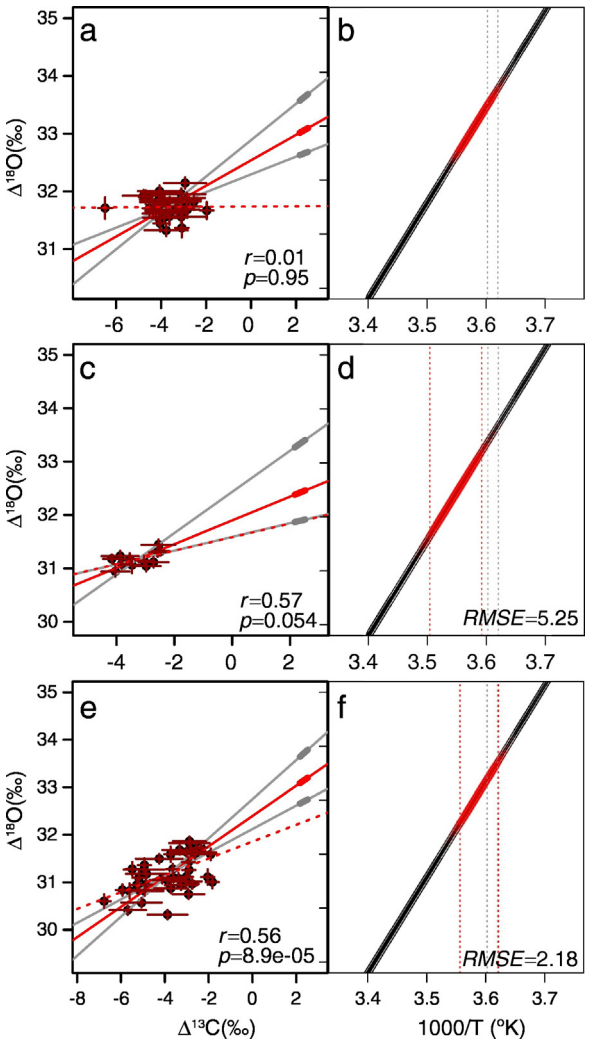

Fig. 7. As in Fig. 6 for AB12-0156 SIMS analyses in a,b) track 1 c,d) track 2 and e,f) track 3. See Fig. 3 for sampling tracks.

terms of temperature (Kim and O'Neil, 1997), these $\delta^{18}O$ would suggest temperatures of 7.1 to 10.4 °C for AB13-0005 and 6.9 to 15.1 °C for AB12-0156.

The strength of linear correlations varied, with significant ($p < 0.05$) relationships in AB13-0005 ($r = 0.32$, $p = 0.01$) and along the innermost sampling path of AB12-0156 (T3; $r = 0.56$, $p \ll 0.001$) (Fig. 3). The next track concentrically inside the outer rim of AB12-0156 showed a marginally significant positive correlation (T2; $r = 0.57$, $p = 0.05$), while the outermost track did not show a significant correlation (T1; $r = 0.01$, $p = 0.9$) (Figs.s 3, 7). Weaker correlation between $\Delta^{13}C$ and $\Delta^{18}O$ produced larger differences in the slope of model I and II regressions. However, the slopes of significant SIMS-based model II relationships overlapped within error of those of milled data (Table 2).

3.3. Δ_{47} data

Mean AB12-0156 and AB13-0005 Δ_{47} values of 0.656 ± 0.011 and 0.663 ± 0.020 (1 se, n = 3), respectively, overlapped within error (Table 3). When interpreted solely in terms of temperature using a comprehensive calibration generated under identical laboratory conditions (Kelson et al., 2017), these Δ_{47} values are equivalent to temperatures of 10.6 ± 3.2 °C and 8.8 ± 5.3 °C for AB12-0156 and AB13-0005, respectively. Although the AB13-0005 temperature overlaps with observations within relatively large error bounds, that for AB12-0156 does not, and both values suggest a subtle warm bias.

3.4. $\delta^{11}B$ data

The $\delta^{11}B$ of AB12-0156 and AB13-0005 were 15.52 ± 0.23 (2 se, n = 6) and 14.37 ± 0.23 (2 se, n = 5), respectively, and do not overlap within error (Table 3). Assuming the parameters described in Section 2.5 are applicable to each coral's site, these values suggest apparent pH values of 7.99 ± 0.05 and 7.79 ± 0.07, respectively. Both pH estimates are

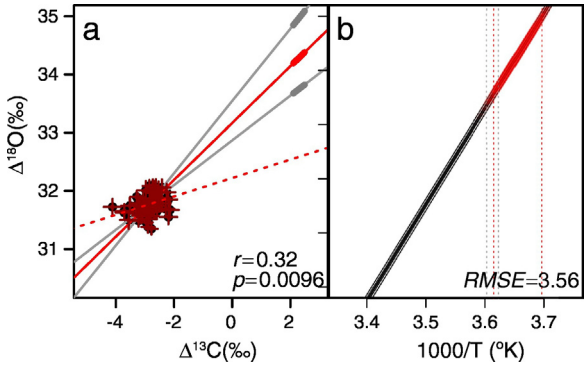

Fig. 8. As in Fig. 6 for AB13-0005 SIMS analyses. See Fig. 4 for sampling track.

Table 3
Δ_{47} and $\delta^{11}B$ results.

ID	$\delta^{18}O$ (‰ PDB)	$\delta^{18}O$ Std. error (‰ PDB)	$\Delta^{18}O$ (‰)	Δ_{47} (‰)	Δ_{47} Std. error (‰)	$\delta^{11}B$ (‰)	$\delta^{11}B$ Std. error (‰)	Apparent pH	Apparent pH Std. error
AB12-0156	0.31	0.20	30.94	0.656	0.011	15.52	0.14	7.99	0.05
AB13-0005	0.81	0.09	31.43	0.663	0.020	14.37	0.12	7.79	0.07

significantly higher than the 7.54 ± 0.07 observed in seawater near collection sites.

4. Discussion

4.1. Potential for reconstructing timeseries

Consistent with previous work, we find strong linear $\Delta^{13}C$ - $\Delta^{18}O$ trends within skeleton deposited over the same time period that are similar to trends in bulk skeleton (Hill et al., 2011; Kimball et al., 2014). Despite a relatively small number of samples from each specimen, milled data suggest that the method of Saenger and Watkins, 2016 may be capable of generating paleotemperature reconstructions with errors of <2 °C when it is reasonable to assume that seawater $\delta^{18}O$ was invariant.

Although this uncertainty is likely too large to capture many intermediate ocean temperature anomalies, well-positioned corals may record spatiotemporal shifts of sharp temperature gradients. For example, stronger gyre circulation and Kuroshio flow driven by changes in wind stress curl during the 1970s and 1980s produced decadal-scale shoaling of the north Pacific thermocline that cooled 200–400 m temperatures by up to 4 °C (Miller et al., 1998; Miller and Schneider, 2000). Similar subsurface variations have been observed in other basins during the past century (Hazeleger et al., 2001; Houghton, 1996; Vargas-Hernández et al., 2015) and could be instrumental in developing decadal scale climate forecasts (Sutton and Allen, 1997). The magnitude of these anomalies can be resolved by our method, suggesting that bamboo corals from appropriate locations could help constrain the behavior of such variability prior to the 20th century, thereby informing simulations of future change.

Furthermore, smaller errors are likely to be possible given that our milled sampling strategy was designed largely to prove a concept rather than to optimize reconstructed temperatures. Milled data in this study agree well with an empirical relationship between the strength of $\Delta^{13}C$ - $\Delta^{18}O$ trends (i.e. –log *p*) and RMSE (Saenger and Watkins, 2016; Fig. 9), implying that a more robust regression with smaller 95% confidence intervals could reduce temperature errors. The likelihood of producing a very strong linear trend can generally be achieved through a greater number of samples, and 50 or more appear to be required to achieve this precision, but may not necessarily be sufficient.

Sampling at this density using a series of concentric paths within a disk of bamboo coral skeleton would be trivial near the outer rim where the circumference is large. However, it would be increasingly challenging toward the coral's center as that circumference decreased, likely resulting in either a decrease in temporal resolution or an increase in reconstructed temperature uncertainty. It may be possible to avoid this complication by extending sampling to the vertical domain (i.e. sampling a coral cylinder rather than a disk) similar to the approach Kimball et al. (2014), but future work is necessary to confirm this.

The fine sampling that can be achieved by SIMS would also allow $\Delta^{13}C$ - $\Delta^{18}O$ trends to be generated from many samples, even in the smaller circumference central portion of a bamboo skeleton. However, our data suggest this approach may not be fruitful. For example, some skeletal regions (e.g. AB12-0156 T1) do not exhibit significant $\Delta^{13}C$ - $\Delta^{18}O$ trends despite dozens of samples. Although the tendency for $\Delta^{13}C$ - $\Delta^{18}O$ trends to become more robust in AB12-0156 track 2 and track 3 suggest that the weak relationship in track 1 may reflect early diagenesis or a different mode of skeletal growth in surface skeleton, confirming this would require additional tracks concentrically inward.

Excluding AB12-0156 track 1, SIMS based temperatures generally agree with milled values, suggesting they are accurate, but may have higher RMS errors despite often being based on trends with a greater number of samples. As discussed in Section 2.4, this general agreement reflects, in part, similarities in the $\Delta^{13}C$ - $\Delta^{18}O$ slope of SIMS and milled data, which is not influenced by the constant correction applied to SIMS data. Although SIMS data generally follow the same empirical relationship in trend significance (i.e. –log *p*) and RMSE that was observed in milled data (Fig. 9), it appears to be more difficult to achieve very robust linear regressions via SIMS even when many samples are included.

The apparent threshold on the significance of SIMS trends likely stems from the inability to measure $\delta^{13}C$ and $\delta^{18}O$ in exactly the same skeleton that arises because of charging of the sample surface. If the spatial scale of skeletal heterogeneity responsible for linear trends is finer than the 20–25 μm SIMS spot, the complementary $\delta^{18}O$ (or $\delta^{13}C$) value for a $\delta^{13}C$ (or $\delta^{18}O$) measurement inferred through interpolation may not be accurate. Consistent with this possibility, the individual crystals that compose bamboo coral skeleton have been shown to measure only 2–4 μm in length (Noé and Dullo, 2006). Furthermore, any correlated errors that cancel during the simultaneous analysis of milled $\delta^{18}O$ and $\delta^{13}C$ using IRMS, would not do so in SIMS analyses, potentially weakening the significance of $\Delta^{13}C$ - $\Delta^{18}O$ trends. From a practical standpoint, this complication seems to outweigh the spatial resolution gained by SIMS, and micromilling appears to be a more promising means of generating $\Delta^{18}O_{aeq}$ timeseries in bamboo corals.

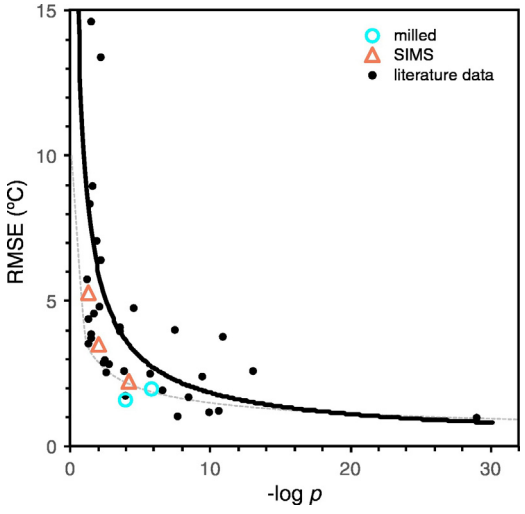

Fig. 9. Relationship between a measure of $\Delta^{13}C$-$\Delta^{18}O$ correlation significance (−log *p*) and RMS error of reconstructed temperature for milled (cyan circles) and SIMS (orange triangles) data. These data agree well with the empirical relationship observed by Saenger and Watkins (2016) in previously published bamboo coral data (bold black line) and the predicted relationship for pseudocorals growing at 4 °C with regression residuals of 0.2‰ (grey dashed line). Literature data from Hill et al. (2011), Kimball et al. (2014) and Farmer et al. (2015a) as presented by Saenger and Watkins (2016). (For interpretation of the references to colour in this figure legend, the reader is referred to the web version of this article.)

4.2. Δ_{47} and $\Delta^{18}O$ insight into vital effects

The Δ_{47} and $\Delta^{18}O$ of bamboo corals are lower than the values expected from abiogenic calcite precipitated from bicarbonate dominated solutions and processed using identical laboratory methods as our bamboo corals (Kelson et al., 2017). Consistent with the Adkins mechanism, the offsets of bamboo coral Δ_{47} and $\Delta^{18}O$ fall on a line connecting HCO_3^- and CO_3^{2-} values (Fig. 10), and are generally similar to recently published results from Gulf of Alaska seamount bamboo corals (Kimball et al., 2015). These data suggest that a biologically-mediated increase of ~0.3–0.5 pH units leads to bamboo coral precipitation from a DIC pool with a higher CO_3^{2-} concentration than the abiogenic experiments on which calibrations are based. Furthermore, AB12-0156, which shows a higher $\delta^{11}B$ value that is consistent with a subtly higher pH, also exhibits lower Δ_{47} and $\Delta^{18}O$ values of the magnitude expected from the shift toward CO_3^{2-} in the Adkins mechanism (Fig. 10). A similar positive Δ_{47} and $\Delta^{18}O$ correlation in *Oculina arbuscula* corals cultured at pH values of 7.5 to 8.1 (Tripati et al., 2015) suggests that pH may also play an important role in generating vital effects in other coral species.

These Δ_{47} and $\Delta^{18}O$ trends are distinct from those of hermatypic surface corals and some aragonitic deep sea corals, which exhibit Δ_{47} that is higher than expected from abiogenic experiments and more consistent with the McConnaughey model (Saenger et al., 2012; Spooner et al., 2016). Multiple factors seem likely to contribute to the difference between surface corals or aragonitic deep sea corals and bamboo corals. Bamboo corals appear to primarily use ambient seawater DIC for calcification, and little to no respired CO_2 is incorporated into their skeletons (Saenger and Watkins, 2016). Because the McConnaughey mechanism suggests that slow hydration/hydroxylation of respired CO_2 produces a disequilibrium DIC pool that is inherited by the coral, the magnitude of its effect will be severely limited when respired CO_2 is a small proportion of all calcifying fluid DIC. Conversely, a greater proportion of the DIC used for calcification in hermatypic surface corals appears to derive from CO_2 (Erez, 1978; Furla et al., 2000). It is more difficult to explain aragonitic deep sea coral data with this argument as available data suggests that they also use very little respired CO_2 for calcification (Adkins et al., 2003).

Rather, the rate of calcification relative to the rate of CO_2 hydration and hydroxylation could also be important. Some aragonitic deep sea corals appear to elevate their calcifying fluid pH to values of ~8.8 (Anagnostou et al., 2012), which is appreciably higher than the 7.8–8.0 we infer for Gulf of Alaska bamboo corals. Although this higher calcifying fluid pH would increase the proportion of carbonate ion, thereby favoring lower Δ_{47} and $\Delta^{18}O$, it would also lead to faster precipitation as well as slower hydration and hydroxylation. Below 5 °C, it takes 1–2 days for DIC to isotopically equilibrate at the pH values we suggest for bamboo corals, and about a week at pH 8.8 (Zeebe and Wolf-Gladrow, 2001). It therefore may be more likely for aragonitic deep sea coral calcification to outpace DIC equilibration, thereby contributing to higher than expected Δ_{47}.

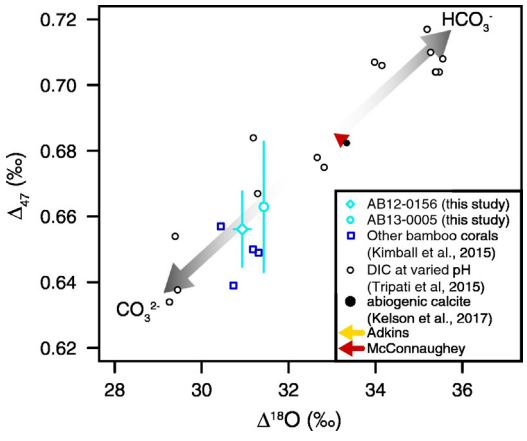

Fig. 10. $\Delta^{18}O$ versus Δ_{47} for AB12-0156 and AB13-0005 (cyan) compared with other Gulf of Alaska bamboo corals (blue open squares; Kimball et al., 2015) and the experimental values for DIC at pH 7.8–12.0 (open black circles; Tripati et al., 2015). AB12-0156 and AB13-0005 exhibit lower and $\Delta^{18}O$ and Δ_{47} than the value expected from abiogenic experiments with identical preparatory, analytical and data reduction protocols (closed black circle; Kelson et al., 2017). The direction and magnitude of $\Delta^{18}O$ versus Δ_{47} trends predicted by the McConnaughey (red) and Adkins (yellow) mechanisms for a 0.5 unit pH upregulation are also shown. The McConnaughey mechanism assumes 4% of the DIC used for calcification derives from respired carbon. See Section 2.7. (For interpretation of the references to colour in this figure legend, the reader is referred to the web version of this article.)

The rate of DIC equilibration will also be affected by the concentration of carbonic anhydrase (CA), an enzyme that catalyzes CO_2 hydration (Uchikawa and Zeebe, 2012), which has been identified in scleractinian and gorgonin corals (Le Goff et al., 2016; Moya et al., 2008). With sufficient concentration, CA could reduce the time necessary for bamboo corals to achieve DIC equilibrium from days to a few minutes (Uchikawa and Zeebe, 2012; Watkins et al., 2013), which would rule out a significant effect from the McConnaughey model. Because CA does not catalyze CO_2 hydroxylation, it would have less of an effect at higher calcifying fluid pH values where the hydroxylation pathway becomes more important (Fig. 5).

These mechanisms are not mutually exclusive, and are probably not exhaustive. However, lower than expected Δ_{47} and $\Delta^{18}O$ in our bamboo corals and Tripati et al.'s (2015) *Oculina arbuscula* suggest these organisms calcify from an equilibrated DIC pool at a pH that is modestly elevated above ambient values in the presence of CA. In contrast, the negative Δ_{47} and $\Delta^{18}O$ trends observed in surface corals (Saenger et al., 2012) and some aragonitic deep sea corals (Spooner et al., 2016) could indicate greater DIC disequilibrium, possibly due to a greater respired CO_2 contribution, higher calcifying fluid pH, faster precipitation rate and/or lower CA concentration.

Although pH up-regulation likely contributes to bamboo coral oxygen and carbon isotope vital effects, the Adkins mechanism does not perfectly describe Δ_{47} and $\Delta^{18}O$ data. With respect to carbon isotopes, Adkins et al. (2003) suggested that skeleton depleted in ^{13}C resulted from a greater proportion of diffused isotopically light respired CO_2 at the site of calcification. However, the Δ_{47} of respired CO_2 would be appreciably higher than that of equilibrium calcite (Dennis et al., 2011; Wang et al., 2004), while transmembrane CO_2 diffusion would increase both Δ_{47} and $\Delta^{18}O$ (Guo et al., 2012; Saenger et al., 2012; Thiagarajan et al., 2011; Tripati et al., 2015) to the degree to which it is represented by Knudsen diffusion. Both processes are therefore generally inconsistent with the lower Δ_{47} we observe.

With respect to oxygen isotopes, Adkins et al. (2003) suggested that the isotopic composition of DIC was directly inherited by the coral skeleton, but this has since been shown not to be the case (Wang et al., 2013; Watkins et al., 2014). Consistent with this, bamboo coral Δ_{47} and $\Delta^{18}O$ are appreciably lower than the HCO_3^- values that approximate the DIC pool at either the pH ~7.5 of Gulf of Alaska seawater (95% HCO_3^-), or the ~7.8–8.0 that may characterize their calcifying fluid (94% HCO_3^-) (Fig. 10). Furthermore, the decrease in Δ_{47} and $\Delta^{18}O$ predicted for a 0.3–0.5 unit upregulation of calcifying fluid pH is only ~0.003‰ and ~0.4‰, respectively, which is much smaller than the difference observed between bamboo corals and abiogenic experiments (Fig. 10). Although the magnitude of Δ_{47} and $\Delta^{18}O$ decrease for a 0.3–0.5 unit upregulation depends on the choice of HCO_3^- and CO_3^{2-} Δ_{47} and $\Delta^{18}O$, which are poorly constrained at the cold temperature of bamboo coral growth, no reasonable choices (Beck et al., 2005; Hill et al., 2014a; Tripati et al., 2015; Wang et al., 2013) approached the difference between corals and abiogenic experiments.

Rather than recording the proportional isotopic composition of DIC, carbonate minerals appear to preferentially inherit the isotopic composition of CO_3^{2-} (Gabitov et al., 2012; Wang et al., 2013). The model of Watkins and Hunt (2015) ostensibly accounts for the effects of pH upregulation on DIC composition as well as the fractionation between

DIC and calcite, and is therefore expected to improve upon Adkins et al. (2003) model. However, the Watkins and Hunt (2015) model still overestimates coral $\Delta^{18}O$. That is, if the Watkins and Hunt (2015) model correctly accounted for all the processes responsible for non-equilibrium isotope signatures in bamboo corals, predicted apparent equilibrium values would closely match coral data and there would be no need to extrapolate trends to more positive apparent equilibrium $\Delta^{13}C$ and $\Delta^{18}O$ (Figs. 6–8). Furthermore, Watkins and Hunt (2015) estimate only a ~0.4‰ $\Delta^{18}O$ decrease between pH 7.5 and 8.0 that is still smaller than that observed between corals and abiogenic experiments.

If it is assumed that the Watkins and Hunt (2015) model accurately represents the abiogenic processes affecting bamboo coral carbon and oxygen isotope fractionation, lower than predicted Δ_{47} and $\Delta^{18}O$ values may reflect biological processes that occur during bamboo coral calcification, but not in abiogenic experiments. That Δ_{47} and $\Delta^{18}O$ fall along the CO_3^{2-} and HCO_3^- trend, suggests that these biological processes may result in bamboo coral calcite inheriting the isotopic signature of CO_3^{2-} in excess of what is predicted. Below we suggest a series of biologically mediated and biologically controlled mechanisms that may contribute to this apparent vital effect. Biologically mediated mechanisms involve biological alteration of the calcifying environment that promotes essentially abiogenic processes capable of generating isotopic disequilibrium, while biologically controlled mechanisms imply that every step of the calcification process is rigorously constrained by biological activity (Saenger and Erez, 2016).

4.2.1. Biologically mediated

Elevation of pH at the site of calcification would favor higher calcite saturation states and faster precipitation (Burton and Walter, 1987), a logical strategy for the often undersaturated growth environments of bamboo corals. In addition to shifts in DIC speciation associated with elevated pH, the Watkins and Hunt (2015) model also considers kinetic effects that may be related to such changes in precipitation rate. This is done at the scale of individual calcium or carbonate ions, and considers fractionations associated with the attachment of aqueous ions to the growing mineral surface, as well as those that occur as mineral-bound ions detach and return to the solution. Biologically mediated processes may be capable of modifying the fractionations that occur during ion attachment and detachment at the fluid-mineral interface, thereby contributing to the coral-model discrepancies discussed above.

Kinetic effects associated with ion attachment and detachment are quantified in the model by carbon and oxygen kinetic fractionation factors (α_f). The value of α_f governs whether a boundary layer at the mineral-fluid interface is enriched or depleted in an isotope relative to the bulk DIC pool. This isotopically distinct mineral-fluid boundary layer is equivalent to those suggested to occur, at least in part, because of the relaxation of the normal calcite lattice structure ~1 nm below the mineral-fluid boundary (Fenter et al., 2000; Rohl et al., 2003). Regardless of whether the boundary layer is considered to be on the mineral or fluid side of the fluid-mineral interface, when growth is slow, calcite is able to achieve its equilibrium isotope composition, but when growth is rapid there is very little isotopic exchange and the surface composition can be entrapped (Gabitov et al., 2012; Watkins et al., 2013, 2014; Watkins and Hunt, 2015; Watson, 2004).

Lower $\Delta^{18}O$ values in faster growing calcite crystals have been used to suggest that the isotopic composition of calcite near the mineral-fluid boundary is depleted in ^{18}O relative to the bulk mineral, consistent with a greater isotopic contribution from CO_3^{2-} relative to other DIC species (Gabitov et al., 2012). This depletion in ^{18}O could not be explained by pH-dependent changes in DIC speciation because the rapid precipitation experiments that produced low $\Delta^{18}O$ values used lower pH fluids than the slow precipitation experiments that yielded high $\Delta^{18}O$ values. If kinetic effects typically produce an ^{18}O depleted mineral-fluid boundary layer, it is not unreasonable to suggest that biologically-mediated processes could alter α_f to generate even greater ^{18}O depletions consistent with the coral-model discrepancies we observe.

Alternatively, or in addition to this effect, biologically-mediated mechanisms may promote greater entrapment of the isotopically distinct boundary layer. However, when typical growth rates over a coral's life span (Farmer et al., 2015b) are extrapolated to the crystal scale, they suggest rates of ~0.003 nm/s, which are appreciably slower than the ~0.1 nm/s where Gabitov et al. (2012) detect kinetic effects, suggesting that crystal scale growth would have to be orders of magnitude faster than bulk skeleton growth, and exhibit long calcification hiatuses, for this possibility to occur.

The concepts above may also contribute to the discrepancies between coral and modelled Δ_{47}. The Watkins and Hunt (2015) model also considers Δ_{47}, and they suggest that the boundary layer described above could also develop a distinct Δ_{47} composition due to the scrambling/unscrambling of isotopologues during transport of ions from the solution to the calcite crystal. This process is assigned the variable ε, with positive values indicating more "clumping" in the boundary layer and negative values less "clumping". When the boundary layer is inherited by the mineral at sufficiently fast precipitation rates, anomalous Δ_{47} values are expected. Tripati et al. (2015) describe, but do not quantify, a very similar mechanism in which distinct boundary layer DIC bond ordering can be inherited by calcite when mineral growth is faster than the time necessary for reordering to achieve equilibrium with the bulk mineral. That bamboo coral Δ_{47} is typically lower than abiogenic experiments and model values implies a near surface region with fewer multiply substituted isotopologues ($\varepsilon < 0$). Whether biologically-mediated processes are capable of generating such a boundary layer remains to be seen.

It is also conceivable that biologically mediated processes encourage calcification through pathways other than those considered by Watkins and Hunt (2015). Wang et al. (2013) propose that solution chemistry and speciation will affect mineral precipitation rate and the rate of isotope exchange. This ultimately affects the pathway through which carbonate is formed, and the degree to which it inherits the isotopic signature of various DIC species. Specifically, they suggest mineral formation through four pathways:

$$Ca^{2+} + CO_3^{2-} \rightleftarrows CaCO_3 \quad (1)$$

$$Ca^{2+} + HCO_3^- \rightleftarrows CaCO_3 + H^+ \quad (2)$$

$$Ca^{2+} + 2HCO_3^- \rightleftarrows CaCO_3 + H_2CO_3 \quad (3)$$

$$Ca^{2+} + HCO_3^- + OH^- \rightleftarrows CaCO_3 + H_2O \quad (4)$$

Pathway (1) is usually energetically most favorable, but at a given temperature, the importance of pathways (2)–(4) increases with pH. The specifics of how precipitation through various pathways affects $\Delta^{18}O$ varies with temperature, salinity, pH and growth rate, but at elevated pH, Wang et al. (2013) suggest that oxygen isotope fractionation decreases at faster precipitation rates, consistent with bamboo coral $\Delta^{18}O$. Because the Watkins and Hunt (2015) model only considers pathways (1) and (2) (Watkins et al., 2014) any biologically mediated process that favors pathways (3) and (4) or alters the expected proportion of skeletogenesis through all four pathways could contribute to bamboo coral vital effects. The degree to which Δ_{47} varies among the pathways above remains to be seen, but will provide important constraints on their ability to explain apparent isotopic disequilibrium.

4.2.2. Biologically controlled

The biologically mediated mechanisms described above rely on bamboo corals promoting calcification by modifying seawater in a closed, or semi-enclosed calcifying space. In contrast to scleractinian corals (Al-Horani et al., 2003; Cai et al., 2016; Venn et al., 2011), it is unknown if bamboo corals possess this isolated environment. Although it is difficult to conceive a mechanism through which pH could be up-regulated in the absence of an isolated space, if one does not exist in

bamboo corals, calcification may be better explained by biologically controlled mechanisms. The most thorough investigation of bamboo coral structure to date, proposed that calcification was highly regulated by an insoluble gorgonin template overlain by a soluble polypeptide sheet of viscous slime (Noé and Dullo, 2006). This polypeptide sheet may control calcification through selective binding of calcium ions, as suggested for some bivalves and sea urchins (Weiner and Addadi, 1991), precipitation of amorphous calcium carbonate (Cuif et al., 2008) or other mechanisms (see Tambutté et al., 2011 for a review).

If biologic processes are able to actively select which ions are, and are not, used to construct bamboo coral skeleton, it is easy to conceive that such a processes could also favor particular carbonate isotopologues, leading to vital effects. That the direction of bamboo coral $\Delta^{18}O$ and Δ_{47} implies greater incorporation of ^{16}O and singly substituted carbonate molecules is not unreasonable given the general preference for light isotopes in other biological processes such as photosynthesis or lipid construction (e.g. Bender, 1971; DeNiro and Epstein, 1977). However, proving that biologically controlled calcification is responsible for bamboo coral vital effects is far from trivial given that their remote growth environments and slow calcification rates are not amenable to either in situ observations or laboratory culture experiments.

4.3. Outlook and future work

The degree to which bamboo coral carbon, oxygen and clumped isotope compositions can be used to reconstruct paleotemperatures and identify biological vital effects using the method of Saenger and Watkins, 2016 and described here, depends in part on how accurately Watkins and Hunt's (2015) model constrains apparent equilibrium. Although we believe our approach is reasonable in its current form and there is no a priori reason to doubt its reliability, a number of variables warrant closer inspection.

The experimental values used to construct Watkins and Hunt's (2015) model are typically based on theoretical calculations (Hill et al., 2014a) and laboratory precipitation experiments (Beck et al., 2005; Dietzel et al., 2009; Kim et al., 2006; Wang et al., 2013; Watkins et al., 2013, 2014) of low Mg calcite that are not the most appropriate analogs for high Mg calcite bamboo corals. It has been suggested that $\Delta^{13}C$ increases as Mg concentration increases in calcites precipitated at 25 °C (Jimenez-Lopez et al., 2006), but this study could not evaluate kinetic effects or temperature dependence. Mavromatis et al. (2012) found that greater Mg substitution did not appreciably change the slope of calcite $\Delta^{18}O$–temperature calibrations, but did systematically increase their intercepts. However, the magnitude of change observed by Mavromatis et al. (2012) does not entirely agree with previous work (Jiménez-López et al., 2004; Tarutani et al., 1969), and no studies have evaluated $\Delta^{18}O$ kinetic effects in high-Mg calcite. To our knowledge there is also no data on Δ_{47} variability in high-Mg calcite precipitated under controlled laboratory conditions. Available data is therefore insufficient to incorporate Mg impurities into Watkins and Hunt's (2015) model at this time, but doing so in the future will be an important modification to the method we describe. Although it is difficult to predict exactly how such a modification would affect our results, it is encouraging that both $\Delta^{18}O$ and $\Delta^{13}C$ increase with Mg substitution. Extrapolating the same coral $\Delta^{18}O$ and $\Delta^{13}C$ trends (e.g. Fig. 6) to a higher $\Delta^{13}C_{aeq}$ would predict a higher $\Delta^{18}O_{aeq}$ that is consistent with the offset intercepts observed by Mavromatis et al. (2012).

Similarly, abiogenic experiments have almost exclusively been conducted at atmospheric pressure. For example, the boron isotope fractionation factor between boric acid and borate ($\alpha_B = 1.0272$) used to calculate pH was experimentally determined at 25 °C, a salinity of 35 and atmospheric pressure (Klochko et al., 2006). The accuracy of $\delta^{11}B$ as a proxy for calcification fluid pH in surface corals growing close to 25 °C is supported by independent pH determinations (Venn et al., 2011), but the equivalent comparison has not been made in deep bamboo corals. Given the wide depth range of bamboo corals, higher pressures and lower temperatures should likely be considered when calculating apparent equilibrium fractionation. Although the pressure dependence of α_B is difficult to predict, a theoretical temperature dependence of $8.2 * 10^{-5}$‰/°C (Zeebe, 2005) would increase α_B to 1.0289 at our coral's ~3.7 °C growth temperature. This modification would increase calculated pH by only a few tenths of a pH unit however, which is too small to explain the $\Delta^{18}O$ discrepancies between bamboo coral $\Delta^{18}O$ and the model of Watkins and Hunt (2015).

Furthermore, the $\Delta^{18}O$ predicted by Watkins and Hunt (2015) at log $R = -7.3$ mol/m^2/s approaches the ~31‰ we measure in bamboo corals only when pH exceeds ~11, which is difficult to explain in terms of uncertainty in α_B. However, it should be noted that the requisite pH drops to a seemingly more realistic ~9.3 when the Watkins and Hunt (2015) model is formulated using experimental HCO_3^- and CO_3^{2-} data (Beck et al., 2005; Tripati et al., 2015) rather than those of Hill et al. (2014a) and Wang et al. (2013). In either case, the model cannot explain the observed coral $\Delta^{18}O$ at any log R value when pH is fixed at 8, suggesting that uncertainties in coral growth rate are unlikely to be the primary source of discrepancies.

Changes in coral growth are still likely to be important however, especially when generating multidecadal and longer timeseries. Bamboo coral radial growth rates can vary through their lifespan (Farmer et al., 2015b), and incorporating such variations into the calculation of $\Delta^{13}C_{aeq}$ will help derive the most accurate $\Delta^{18}O_{aeq}$ possible. However, constraining such changes in growth rate with high precision and over short timescales will remain a challenge unless robust annual banding patterns or regular geochemical cycles suitable for absolute age control can be identified in bamboo corals.

Although we remain optimistic about the potential to extract paleotemperature timeseries using the methods we describe, we acknowledge that future refinements to the $\delta^{11}B$ paleo-pH proxy and the formulation of the Watkins and Hunt (2015) model may require revisions in the future. These revisions are not anticipated to fundamentally change the results obtained from the method in its current form, but may improve its precision, accuracy and ability to distinguish between proposed sources for bamboo coral vital effects.

5. Conclusions

Through high resolution sampling, we demonstrate that bamboo corals exhibit linearly correlated carbon and oxygen isotope variability in approximately coeval skeleton. This correlation can be used to derive accurate estimates of apparent equilibrium oxygen isotope fractionation, which suggests that paleotemperature timeseries may be generated from bamboo corals when the oxygen isotopic composition of seawater can be considered constant. The strength of linear trends is the primary control on reconstructed temperature errors, which are <2 °C for skeleton sampled at a spatial resolution of hundreds of microns via micromill. Furthermore, because our data agree with a previously derived relationship between linear trend significance and reconstructed temperature uncertainty, uncertainty of <1 °C may be possible when robust trends are constrained by dozens of samples.

In contrast to milled samples, trends based on SIMS analyses at spatial scales of tens of microns are weaker, but still sometimes significant. Despite being based on a relatively high number of samples, these trends yield temperature errors of >2 °C suggesting that denser sampling may not necessarily improve SIMS-based temperatures. This is likely related to the inability to measure carbon and oxygen isotopes in exactly the same skeletal region, and may reflect skeletal heterogeneity on spatial scales smaller than SIMS spots or correlated errors that cancel in milled samples measured by IRMS, but not in interpolated SIMS analyses. This limitation suggests that a milled sampling approach is likely the most practical for generating bamboo coral-based paleotemperature timeseries.

Insight into the mechanism(s) responsible for linear trends in carbon and oxygen isotopes is provided by carbonate clumped isotopes.

These data suggest that a previous biomineralization model described by Adkins et al. (2003) better describes bamboo coral calcification compared to that of McConnaughey (1989), but is not a perfect analog. Although the Adkins et al. (2003) model does not perfectly describe bamboo coral vital effects, clumped isotope data suggests that pH is an important variable controlling their magnitude. Processes absent from current biomineralization models that may contribute to vital effects include the entrapment of an isotopically unique boundary layer at the mineral-fluid interface, variations in the chemical pathway through which calcite is precipitated or the role of Mg is calcite-fluid isotopic fractionation.

Future work that evaluates the importance of these mechanisms will be important for accurately estimating apparent equilibrium oxygen isotope fractionation and, in turn, paleotemperature. Similarly, developments in the boron isotope pH proxy and the ability to accurately estimate bamboo coral growth may require refinements to the method of Saenger and Watkins, 2016, and its application to timeseries described here. However, we see no a priori reason why any such refinements should fundamentally change our results, and we remain optimistic on the potential for bamboo corals to yield meaningful timeseries of sub-surface temperature variability.

Acknowledgements

C.S. acknowledges support from the University of Washington School of Oceanography. J.R.F. acknowledges support from the NSF Graduate Research Fellowship Program (DGE-11-44155). We also thank Ming-Chang Liu for help with SIMS isotopic analyses, which were supported by Mississippi State University and the University of Washington, as well as Bärbel Hönisch for access to her boron isotope laboratory. Three anonymous reviews improved the quality of this work.

Appendix A. Supplementary data

Supplementary data to this article can be found online at http://dx.doi.org/10.1016/j.chemgeo.2017.02.014.

References

Adkins, J.F., Boyle, E.A., Curry, W.B., Lutringer, A., 2003. Stable isotopes in deep-sea corals and a new mechanism for "vital effects". Geochim. Cosmochim. Acta 67:1129–1143. http://dx.doi.org/10.1016/S0016-7037(02)01203-6.

Affek, H.P., Bar-Matthews, M., Ayalon, A., Matthews, A., Eiler, J.M., 2008. Glacial/interglacial temperature variations in Soreq cave speleothems as recorded by "clumped isotope" thermometry. Geochim. Cosmochim. Acta 72:5351–5360. http://dx.doi.org/10.1016/j.gca.2008.06.031.

Al-Horani, F.A., Al-Moghrabi, S.M., de Beer, D., 2003. The mechanism of calcification and its relation to photosynthesis and respiration in the scleractinian coral *Galaxea fascicularis*. Mar. Biol. 142:419–426. http://dx.doi.org/10.1007/s00227-002-0981-8.

Anagnostou, E., Huang, K.-F., You, C.-F., Sikes, E.L., Sherrell, R.M., 2012. Evaluation of boron isotope ratio as a pH proxy in the deep sea coral *Desmophyllum dianthus*: evidence of physiological pH adjustment. Earth Planet. Sci. Lett. 349–350:251–260. http://dx.doi.org/10.1016/j.epsl.2012.07.006.

Andrews, A.H., Stone, R.P., Lundstrom, C.C., DeVogelaere, A.P., 2009. Growth rate and age determination of bamboo corals from the northeastern Pacific Ocean using refined ^{210}Pb dating. Mar. Ecol. Prog. Ser. 397:173–185. http://dx.doi.org/10.3354/meps08193.

Beck, W.C., Grossman, E.L., Morse, J.W., 2005. Experimental studies of oxygen isotope fractionation in the carbonic acid system at 15°, 25°, and 40 °C. Geochim. Cosmochim. Acta 69:3493–3503. http://dx.doi.org/10.1016/j.gca.2005.02.003.

Bender, M.M., 1971. Variations in the $^{13}C/^{12}C$ ratios of plants in relation to the pathway of photosynthetic carbon dioxide fixation. Phytochemistry 10:1239–1244. http://dx.doi.org/10.1016/S0031-9422(00)84324-1.

Blamart, D., Rollion-Bard, C., Cuif, J.-P., Juillet-Leclerc, A., Lutringer, A., van Weering, T.C.E., Henriet, J.-P., 2005. C and O isotopes in a deep-sea coral (*Lophelia pertusa*) related to skeletal microstructure. In: Freiwald, P.D.A., Roberts, D.J.M. (Eds.), Cold-water Corals and Ecosystems. Erlangen Earth Conference Series. Springer, Berlin Heidelberg, pp. 1005–1020.

Brand, W.A., Assonov, S.S., Coplen, T.B., 2010. Correction for the 17O interference in $\delta(^{13}C)$ measurements when analyzing CO_2 with stable isotope mass spectrometry (IUPAC Technical Report). Pure Appl. Chem. 82:1719–1733. http://dx.doi.org/10.1351/PAC-REP-09-01-05.

Burton, E.A., Walter, L.M., 1987. Relative precipitation rates of aragonite and Mg calcite from seawater: Temperature or carbonate ion control? Geology 15:111–114. http://dx.doi.org/10.1130/0091-7613(1987)15<111:RPROAA>2.0.CO;2.

Cai, W.-J., Ma, Y., Hopkinson, B.M., Grottoli, A.G., Warner, M.E., Ding, Q., Hu, X., Yuan, X., Schoepf, V., Xu, H., Han, C., Melman, T.F., Hoadley, K.D., Pettay, D.T., Matsui, Y., Baumann, J.H., Levas, S., Ying, Y., Wang, Y., 2016. Microelectrode characterization of coral daytime interior pH and carbonate chemistry. Nat. Commun. 7:11144. http://dx.doi.org/10.1038/ncomms11144.

Capotondi, A., Alexander, M.A., Bond, N.A., Curchitser, E.N., Scott, J.D., 2012. Enhanced upper ocean stratification with climate change in the CMIP3 models. J. Geophys. Res. 117, C04031. http://dx.doi.org/10.1029/2011JC007409.

Chen, X., Tung, K.-K., 2014. Varying planetary heat sink led to global-warming slowdown and acceleration. Science 345:897–903. http://dx.doi.org/10.1126/science.1254937.

Collins, M., An, S.-I., Cai, W., Ganachaud, A., Guilyardi, E., Jin, F.-F., Jochum, M., Lengaigne, M., Power, S., Timmermann, A., Vecchi, G., Wittenberg, A., 2010. The impact of global warming on the tropical Pacific Ocean and El Niño. Nat. Geosci. 3:391–397. http://dx.doi.org/10.1038/ngeo868.

Coplen, T.B., 2007. Calibration of the calcite–water oxygen-isotope geothermometer at Devils Hole, Nevada, a natural laboratory. Geochim. Cosmochim. Acta 71:3948–3957. http://dx.doi.org/10.1016/j.gca.2007.05.028.

Cuif, J.P., Dauphin, Y., Farre, B., Nehrke, G., Nouet, J., Salomé, M., 2008. Distribution of sulphated polysaccharides within calcareous biominerals suggests a widely shared two-step crystallization process for the microstructural growth units. Mineral. Mag. 72:233–237. http://dx.doi.org/10.1180/minmag.2008.072.1.233.

Defliese, W.F., Hren, M.T., Lohmann, K.C., 2015. Compositional and temperature effects of phosphoric acid fractionation on Δ47 analysis and implications for discrepant calibrations. Chem. Geol. http://dx.doi.org/10.1016/j.chemgeo.2014.12.018.

DeNiro, M.J., Epstein, S., 1977. Mechanism of carbon isotope fractionation associated with lipid synthesis. Science 197, 261–263.

Dennis, K.J., Affek, H.P., Passey, B.H., Schrag, D.P., Eiler, J.M., 2011. Defining an absolute reference frame for "clumped" isotope studies of CO2. Geochim. Cosmochim. Acta 75:7117–7131. http://dx.doi.org/10.1016/j.gca.2011.09.025.

Dewitte, B., Yeh, S.-W., Thual, S., 2012. Reinterpreting the thermocline feedback in the western-central equatorial Pacific and its relationship with the ENSO modulation. Clim. Dyn. 41:819–830. http://dx.doi.org/10.1007/s00382-012-1504-z.

Dickson, A.G., 1990. Thermodynamics of the dissociation of boric acid in synthetic seawater from 273.15 to 318.15 K. Deep Sea Res. Part A 37:755–766. http://dx.doi.org/10.1016/0198-0149(90)90004-F.

Dietzel, M., Tang, J., Leis, A., Köhler, S.J., 2009. Oxygen isotopic fractionation during inorganic calcite precipitation — effects of temperature, precipitation rate and pH. Chem. Geol. 268:107–115. http://dx.doi.org/10.1016/j.chemgeo.2009.07.015.

Eiler, J.M., 2007. "Clumped-isotope" geochemistry—the study of naturally-occurring, multiply-substituted isotopologues. Earth Planet. Sci. Lett. 262:309–327. http://dx.doi.org/10.1016/j.epsl.2007.08.020.

Erez, J., 1978. Vital effect on stable-isotope composition seen in foraminifera and coral skeletons. Nature 273:199–202. http://dx.doi.org/10.1038/273199a0.

Etnoyer, P., Morgan, L.E., 2005. Habitat-forming deep-sea corals in the Northeast Pacific Ocean. In: Freiwald, P.D.A., Roberts, D.J.M. (Eds.), Cold-Water Corals and Ecosystems. Erlangen Earth Conference Series. Springer, Berlin Heidelberg:pp. 331–343 http://dx.doi.org/10.1007/3-540-27673-4_16.

Farmer, J.R., Hönisch, B., Robinson, L.F., Hill, T.M., 2015a. Effects of seawater-pH and biomineralization on the boron isotopic composition of deep-sea bamboo corals. Geochim. Cosmochim. Acta 155:86–106. http://dx.doi.org/10.1016/j.gca.2015.01.018.

Farmer, J.R., Robinson, L.F., Hönisch, B., 2015b. Growth rate determinations from radiocarbon in bamboo corals (genus *Keratoisis*). Deep-Sea Res. I Oceanogr. Res. Pap. 105:26–40. http://dx.doi.org/10.1016/j.dsr.2015.08.004.

Fayek, M., Harrison, T.M., Ewing, R.C., Grove, M., Coath, C.D., 2002. O and Pb isotopic analyses of uranium minerals by ion microprobe and U–Pb ages from the Cigar Lake deposit. Chem. Geol. 185:205–225. http://dx.doi.org/10.1016/S0009-2541(01)00401-6.

Fenter, P., Geissbühler, P., DiMasi, E., Srajer, G., Sorensen, L.B., Sturchio, N.C., 2000. Surface speciation of calcite observed in situ by high-resolution X-ray reflectivity. Geochim. Cosmochim. Acta 64:1221–1228. http://dx.doi.org/10.1016/S0016-7037(99)00403-2.

Foster, G.L., Pogge von Strandmann, P.a.E., Rae, J.W.B., 2010. Boron and magnesium isotopic composition of seawater. Geochem. Geophys. Geosyst. 11, Q08015. http://dx.doi.org/10.1029/2010GC003201.

Furla, P., Galgani, I., Durand, I., Allemand, D., 2000. Sources and mechanisms of inorganic carbon transport for coral calcification and photosynthesis. J. Exp. Biol. 203, 3445–3457.

Gabitov, R.I., Watson, E.B., Sadekov, A., 2012. Oxygen isotope fractionation between calcite and fluid as a function of growth rate and temperature: an in situ study. Chem. Geol. 306–307:92–102. http://dx.doi.org/10.1016/j.chemgeo.2012.02.021.

Grossman, E.L., Ku, T.-L., 1986. Oxygen and carbon isotope fractionation in biogenic aragonite: Temperature effects. Chem. Geol. Isot. Geosci. 59:59–74 Calibration of the Phanerozoic Time Scale. 10.1016/0168-9622(86)90057-6.

Guo, W., Kim, S.T., Yuan, J., Farquhar, J., Passey, B.H., 2012. ^{13}C-^{18}O bonds in dissovled inorganic carbon: toward a better understanding of clumped isotope thermometer in biogenic carbonates. Mineralogical Magazine. Presented at the Goldschmidt, p. 1791.

Hazeleger, W., Visbeck, M., Cane, M., Karspeck, A., Naik, N., 2001. Decadal upper ocean temperature variability in the tropical Pacific. J. Geophys. Res. 106:8971–8988. http://dx.doi.org/10.1029/2000JC000536.

He, B., Olack, G.A., Colman, A.S., 2012. Pressure baseline correction and high-precision CO_2 clumped-isotope (Δ_{47}) measurements in bellows and micro-volume modes. Rapid Commun. Mass Spectrom. 26:2837–2853. http://dx.doi.org/10.1002/rcm.6436.

Hemming, N.G., Hanson, G.N., 1994. A procedure for the isotopic analysis of boron by negative thermal ionization mass spectrometry. Chem. Geol. 114:147–156. http://dx.doi.org/10.1016/0009-2541(94)90048-5.

Hill, T.M., Spero, H.J., Guilderson, T., LaVigne, M., Clague, D., Macalello, S., Jang, N., 2011. Temperature and vital effect controls on bamboo coral (*Isididae*) isotope geochemistry: A test of the "lines method". Geochem. Geophys. Geosyst. 12, Q04008. http://dx.doi.org/10.1029/2010GC003443.

Hill, T.M., LaVigne, M., Spero, H.J., Guilderson, T., Gaylord, B., Clague, D., 2012. Variations in seawater Sr/Ca recorded in deep-sea bamboo corals. Paleoceanography 27, PA3202. http://dx.doi.org/10.1029/2011PA002260.

Hill, T.M., Myrvold, C.R., Spero, H.J., Guilderson, T.P., 2014a. Evidence for benthic–pelagic food web coupling and carbon export from California margin bamboo coral archives. Biogeosciences 11:3845–3854. http://dx.doi.org/10.5194/bg-11-3845-2014.

Hill, P.S., Tripati, A.K., Schauble, E.A., 2014b. Theoretical constraints on the effects of pH, salinity, and temperature on clumped isotope signatures of dissolved inorganic carbon species and precipitating carbonate minerals. Geochim. Cosmochim. Acta 125: 610–652. http://dx.doi.org/10.1016/j.gca.2013.06.018.

Houghton, R.W., 1996. Subsurface quasi-decadal fluctuations in the North Atlantic. J. Clim. 9:1363–1373. http://dx.doi.org/10.1175/1520-0442(1996)009<1363:SQDFIT>2.0.CO;2.

Jiménez-López, C., Romanek, C.S., Huertas, F.J., Ohmoto, H., Caballero, E., 2004. Oxygen isotope fractionation in synthetic magnesian calcite. Geochim. Cosmochim. Acta 68: 3367–3377. http://dx.doi.org/10.1016/j.gca.2003.11.033.

Jimenez-Lopez, C., Romanek, C.S., Caballero, E., 2006. Carbon isotope fractionation in synthetic magnesian calcite. Geochim. Cosmochim. Acta 70:1163–1171. http://dx.doi.org/10.1016/j.gca.2005.11.005.

Kelson, J.R., Huntington, K.W., Schauer, A.J., Saenger, C., Lechler, A.R., 2017. Toward a universal carbonate clumped isotope calibration: diverse synthesis and preparatory methods suggest a single temperature relationship. Geochim. Cosmochim. Acta 197:104–131. http://dx.doi.org/10.1016/j.gca.2016.10.010.

Kim, S.-T., O'Neil, J.R., 1997. Equilibrium and nonequilibrium oxygen isotope effects in synthetic carbonates. Geochim. Cosmochim. Acta 61:3461–3475. http://dx.doi.org/10.1016/S0016-7037(97)00169-5.

Kim, S.-T., Hillaire-Marcel, C., Mucci, A., 2006. Mechanisms of equilibrium and kinetic oxygen isotope effects in synthetic aragonite at 25 °C. Geochim. Cosmochim. Acta 70:5790–5801 A Special Issue Dedicated to Robert A. Berner. 10.1016/j.gca.2006.08.003.

Kim, S.-T., Gebbinck, C.K., Mucci, A., Coplen, T.B., 2014. Oxygen isotope systematics in the aragonite–CO_2–H_2O–NaCl system up to 0.7 mol/kg ionic strength at 25 °C. Geochim. Cosmochim. Acta 137:147–158. http://dx.doi.org/10.1016/j.gca.2014.02.050.

Kimball, J.B., Dunbar, R.B., Guilderson, T.P., 2014. Oxygen and carbon isotope fractionation in calcitic deep-sea corals: Implications for paleotemperature reconstruction. Chem. Geol. 381:223–233. http://dx.doi.org/10.1016/j.chemgeo.2014.05.008.

Kimball, J., Tripati, R.E., Dunbar, R., 2015. Carbonate "clumped" isotope signatures in aragonitic scleractinian and calcitic gorgonian deep-sea corals. Biogeosci. Discuss. 2015: 19115–19165. http://dx.doi.org/10.5194/bgd-12-19115-2015.

Klochko, K., Kaufman, A.J., Yao, W., Byrne, R.H., Tossell, J.A., 2006. Experimental measurement of boron isotope fractionation in seawater. Earth Planet. Sci. Lett. 248:276–285. http://dx.doi.org/10.1016/j.epsl.2006.05.034.

Kluge, T., Affek, H.P., Zhang, Y.G., Dublyansky, Y., Spötl, C., Immenhauser, A., Richter, D.K., 2014. Clumped isotope thermometry of cryogenic cave carbonates. Geochim. Cosmochim. Acta 126:541–554. http://dx.doi.org/10.1016/j.gca.2013.11.011.

LaVigne, M., Hill, T.M., Spero, H.J., Guilderson, T.P., 2011. Bamboo coral Ba/Ca: calibration of a new deep ocean refractory nutrient proxy. Earth Planet. Sci. Lett. 312:506–515. http://dx.doi.org/10.1016/j.epsl.2011.10.013.

Le Goff, C.L., Ganot, P., Zoccola, D., Caminiti-Segonds, N., Allemand, D., Tambutté, S., 2016. Carbonic anhydrases in cnidarians: novel perspectives from the octocorallian *Corallium rubrum*. PLoS One 11, e0160368. http://dx.doi.org/10.1371/journal.pone.0160368.

LeGrande, A.N., Schmidt, G.A., 2006. Global gridded data set of the oxygen isotopic composition in seawater. Geophys. Res. Lett. 33, L12604. http://dx.doi.org/10.1029/2006GL026011.

Li, G., Xie, S.-P., Du, Y., 2015. Climate model errors over the South Indian Ocean thermocline dome and their effect on the basin mode of interannual variability. J. Clim. 28: 3093–3098. http://dx.doi.org/10.1175/JCLI-D-14-00810.1.

Locarnini, R.A., Mishonov, A.V., Antonov, J.I., Boyer, T.P., Garcia, H.E., Baranova, O.K., Zweng, M.M., Johnson, D.R., 2010. World Ocean Atlas 2009, volume 1: temperature. NOAA Atlas NESDIS 68. U.S. Government Printing Office, Washington D.C., p. 184.

Mavromatis, V., Schmidt, M., Botz, R., Comas-Bru, L., Oelkers, E.H., 2012. Experimental quantification of the effect of Mg on calcite–aqueous fluid oxygen isotope fractionation. Chem. Geol. 310–311:97–105. http://dx.doi.org/10.1016/j.chemgeo.2012.03.027.

McConnaughey, T., 1989. ^{13}C and ^{18}O isotopic disequilibrium in biological carbonates: I. Patterns. Geochim. Cosmochim. Acta 53:151–162. http://dx.doi.org/10.1016/0016-7037(89)90282-2.

McConnaughey, T.A., 2003. Sub-equilibrium oxygen-18 and carbon-13 levels in biological carbonates: carbonate and kinetic models. Coral Reefs 22:316–327. http://dx.doi.org/10.1007/s00338-003-0325-2.

McCrea, J.M., 1950. On the isotopic chemistry of carbonates and a paleotemperature scale. J. Chem. Phys. 18:849–857. http://dx.doi.org/10.1063/1.1747785.

McDonagh, E.L., Bryden, H.L., King, B.A., Sanders, R.J., Cunningham, S.A., Marsh, R., 2005. Decadal changes in the South Indian Ocean thermocline. J. Clim. 18:1575–1590. http://dx.doi.org/10.1175/JCLI3350.1.

Miller, A.J., Schneider, N., 2000. Interdecadal climate regime dynamics in the North Pacific Ocean: theories, observations and ecosystem impacts. Prog. Oceanogr. 47:355–379. http://dx.doi.org/10.1016/S0079-6611(00)00044-6.

Miller, A.J., Cayan, D.R., White, W.B., 1998. A westward-intensified decadal change in the North Pacific thermocline and gyre-scale circulation. J. Clim. 11:3112–3127. http://dx.doi.org/10.1175/1520-0442(1998)011<3112:AWIDCI>2.0.CO;2.

Moya, A., Tambutté, S., Bertucci, A., Tambutté, E., Lotto, S., Vullo, D., Supuran, C.T., Allemand, D., Zoccola, D., 2008. Carbonic anhydrase in the scleractinian coral *Stylophora pistillata*: characterization, localization, and role in biomineralization. J. Biol. Chem. 283:25475–25484. http://dx.doi.org/10.1074/jbc.M804726200.

Noé, S.U., Dullo, W.-C., 2006. Skeletal morphogenesis and growth mode of modern and fossil deep-water isidid gorgonians (Octocorallia) in the West Pacific (New Zealand and Sea of Okhotsk). Coral Reefs 25:303–320. http://dx.doi.org/10.1007/s00338-006-0095-8.

O'Neil, J.R., Clayton, R.N., Mayeda, T.K., 1969. Oxygen isotope fractionation in divalent metal carbonates. J. Chem. Phys. 51:5547–5558. http://dx.doi.org/10.1063/1.1671982.

Peters, N.A., Huntington, K.W., Hoke, G.D., 2013. Hot or not? Impact of seasonally variable soil carbonate formation on paleotemperature and O-isotope records from clumped isotope thermometry. Earth Planet. Sci. Lett. 361:208–218. http://dx.doi.org/10.1016/j.epsl.2012.10.024.

Prouty, N.G., Roark, E.B., Andrews, A., Robinson, L., Hill, T., Sherwood, O., Williams, B., Guilderson, T., Fallon, S., 2015. Age, growth rates, and paleoclimate studies. The State of Deep-Sea Coral and Sponge Ecosystems of the United States: 2015, NOAA Technical Memorandum X. NOAA, Silver Spring, pp. 1–21.

Ramesh, N., Murtugudde, R., 2013. All flavours of El Nino have similar early subsurface origins. Nat. Clim. Chang. 3:42–46. http://dx.doi.org/10.1038/nclimate1600.

Rao, S.A., Behera, S.K., Masumoto, Y., Yamagata, T., 2002. Interannual subsurface variability in the tropical Indian Ocean with a special emphasis on the Indian Ocean Dipole. Deep-Sea Res. II Top. Stud. Oceanogr. 49:1549–1572 World Ocean Circulation Experiment. 10.1016/S0967-0645(01)00158-8.

Roark, E.B., Guilderson, T.P., Flood-Page, S., Dunbar, R.B., Ingram, B.L., Fallon, S.J., McCulloch, M., 2005. Radiocarbon-based ages and growth rates of bamboo corals from the Gulf of Alaska. Geophys. Res. Lett. 32, L04606. http://dx.doi.org/10.1029/2004GL021919.

Robinson, L.F., Adkins, J.F., Frank, N., Gagnon, A.C., Prouty, N.G., Brendan Roark, E., van de Flierdt, T., 2014. The geochemistry of deep-sea coral skeletons: a review of vital effects and applications for palaeoceanography. Deep-Sea Res. II Top. Stud. Oceanogr. 99:184–198 Biology and Geology of Deep-Sea Coral Ecosystems: Proceedings of the Fifth International Symposium on Deep Sea Corals. 10.1016/j.dsr2.2013.06.005.

Rohl, A.L., Wright, K., Gale, J.D., 2003. Evidence from surface phonons for the (2×1) reconstruction of the (1014) surface of calcite from computer simulation. Am. Mineral. 88, 921–925.

Rollion-Bard, C., Marin-Carbonne, J., 2011. Determination of SIMS matrix effects on oxygen isotopic compositions in carbonates. J. Anal. At. Spectrom. 26:1285–1289. http://dx.doi.org/10.1039/C0JA00213E.

Rollion-Bard, C., Blamart, D., Cuif, J.-P., Juillet-Leclerc, A., 2003a. Microanalysis of C and O isotopes of azooxanthellate and zooxanthellate corals by ion microprobe. Coral Reefs 22:405–415. http://dx.doi.org/10.1007/s00338-003-0347-9.

Rollion-Bard, C., Chaussidon, M., France-Lanord, C., 2003b. pH control on oxygen isotopic composition of symbiotic corals. Earth Planet. Sci. Lett. 215:275–288. http://dx.doi.org/10.1016/S0012-821X(03)00391-1.

Rollion-Bard, C., Blamart, D., Cuif, J.-P., Dauphin, Y., 2010. In situ measurements of oxygen isotopic composition in deep-sea coral, *Lophelia pertusa*: re-examination of the current geochemical models of biomineralization. Geochim. Cosmochim. Acta 74: 1338–1349. http://dx.doi.org/10.1016/j.gca.2009.11.011.

Saenger, C., Affek, H.P., Felis, T., Thiagarajan, N., Lough, J.M., Holcomb, M., 2012. Carbonate clumped isotope variability in shallow water corals: temperature dependence and growth-related vital effects. Geochim. Cosmochim. Acta 99:224–242. http://dx.doi.org/10.1016/j.gca.2012.09.035.

Saenger, C., Watkins, J.M., 2016. A refined method for calculating paleotemperatures from linear correlations in bamboo coral carbon and oxygen isotopes. Paleoceanography 31. http://dx.doi.org/10.1002/2016PA002931 2016PA002931.

Saenger, C., Erez, J., 2016. A Non-traditional Stable Isotope Perspective on Coral Calcification. In: Goffredo, S., Dubinsky, Z. (Eds.), The Cnidaria, Past, Present and Future. Springer International Publishing:pp. 181–205 http://dx.doi.org/10.1007/978-3-319-31305-4_12.

Schauer, A.J., Kelson, J., Saenger, C., Huntington, K.W., 2016. Choice of ^{17}O correction affects clumped isotope (Δ_{47}) values of CO_2 measured with mass spectrometry. Rapid Commun. Mass Spectrom. n/a-n/a. 10.1002/rcm.7743.

Sherwood, O.A., Edinger, E.N., 2009. Ages and growth rates of some deep-sea gorgonian and antipatharian corals of Newfoundland and Labrador. Can. J. Fish. Aquat. Sci. 66, 142–152.

Smith, J.E., Schwarcz, H.P., Risk, M.J., McCONNAUGHEY, T.A., Keller, N., 2000. Paleotemperatures from deep-sea corals: overcoming "vital effects". PALAIOS 15: 25–32. http://dx.doi.org/10.1669/0883-1351(2000)015<0025:PFDSCO>2.0.CO;2.

Spooner, P.T., Guo, W., Robinson, L.F., Thiagarajan, N., Hendry, K.R., Rosenheim, B.E., Leng, M.J., 2016. Clumped isotope composition of cold-water corals: a role for vital effects? Geochim. Cosmochim. Acta 179:123–141. http://dx.doi.org/10.1016/j.gca.2016.01.023.

Stone, R.P., 2014. The ecology of deep-sea coral and sponge habitats of the central Aleutian Islands of Alaska. NOAA Professional Paper NMFS 16:52. http://dx.doi.org/10.7755/PP.16.

Sutton, R.T., Allen, M.R., 1997. Decadal predictability of North Atlantic sea surface temperature and climate. Nature 388:563–567. http://dx.doi.org/10.1038/41523.

Tambutté, S., Holcomb, M., Ferrier-Pagès, C., Reynaud, S., Tambutté, É., Zoccola, D., Allemand, D., 2011. Coral biomineralization: from the gene to the environment. J. Exp. Mar. Biol. Ecol. 408:58–78 Coral Reefs: Future Directions. 10.1016/j.jembe.2011.07.026.

Tarutani, T., Clayton, R.N., Mayeda, T.K., 1969. The effect of polymorphism and magnesium substitution on oxygen isotope fractionation between calcium carbonate and water. Geochim. Cosmochim. Acta 33:987–996. http://dx.doi.org/10.1016/0016-7037(69)90108-2.

Thiagarajan, N., Adkins, J., Eiler, J., 2011. Carbonate clumped isotope thermometry of deep-sea corals and implications for vital effects. Geochim. Cosmochim. Acta 75: 4416–4425. http://dx.doi.org/10.1016/j.gca.2011.05.004.

Thompson, L.A., Cheng, W., 2008. Water masses in the Pacific in CCSM3. J. Clim. 21: 4514–4528. http://dx.doi.org/10.1175/2008JCLI2280.1.

Thresher, R.E., Neil, H., 2016. Scale dependence of environmental and physiological correlates of $\delta^{18}O$ and $\delta^{13}C$ in the magnesium calcite skeletons of bamboo corals (Gorgonacea; Isididae). Geochim. Cosmochim. Acta 187:260–278. http://dx.doi.org/10.1016/j.gca.2016.05.024.

Thresher, R., Rintoul, S.R., Koslow, J.A., Weidman, C., Adkins, J., Proctor, C., 2004. Oceanic evidence of climate change in southern Australia over the last three centuries. Geophys. Res. Lett. 31, L07212. http://dx.doi.org/10.1029/2003GL018869.

Thresher, R.E., MacRae, C.M., Wilson, N.C., Gurney, R., 2007. Environmental effects on the skeletal composition of deep-water gorgonians (*Keratoisis* spp.; Isididae). Bull. Mar. Sci. 81, 409–422.

Thresher, R.E., MacRae, C.M., Wilson, N.C., Fallon, S., 2009. Feasibility of age determination of deep-water bamboo corals (Gorgonacea; Isididae) from annual cycles in skeletal composition. Deep-Sea Res. I Oceanogr. Res. Pap. 56:442–449. http://dx.doi.org/10.1016/j.dsr.2008.10.003.

Thresher, R.E., Wilson, N.C., MacRae, C.M., Neil, H., 2010. Temperature effects on the calcite skeletal composition of deep-water gorgonians (Isididae). Geochim. Cosmochim. Acta 74:4655–4670. http://dx.doi.org/10.1016/j.gca.2010.05.024.

Tobin, T.S., Schauer, A.J., Lewarch, E., 2011. Alteration of micromilled carbonate $\delta^{18}O$ during Kiel Device analysis. Rapid Commun. Mass Spectrom. 25, 2149–2152.

Tripati, A.K., Hill, P.S., Eagle, R.A., Mosenfelder, J.L., Tang, J., Schauble, E.A., Eiler, J.M., Zeebe, R.E., Uchikawa, J., Coplen, T.B., Ries, J.B., Henry, D., 2015. Beyond temperature: clumped isotope signatures in dissolved inorganic carbon species and the influence of solution chemistry on carbonate mineral composition. Geochim. Cosmochim. Acta 166:344–371. http://dx.doi.org/10.1016/j.gca.2015.06.021.

Uchikawa, J., Zeebe, R.E., 2012. The effect of carbonic anhydrase on the kinetics and equilibrium of the oxygen isotope exchange in the CO_2–H_2O system: implications for $\delta^{18}O$ vital effects in biogenic carbonates. Geochim. Cosmochim. Acta 95:15–34. http://dx.doi.org/10.1016/j.gca.2012.07.022.

Usdowski, E., Hoefs, J., 1993. Oxygen isotope exchange between carbonic acid, bicarbonate, carbonate, and water: a re-examination of the data of McCrea (1950) and an expression for the overall partitioning of oxygen isotopes between the carbonate species and water. Geochim. Cosmochim. Acta 57:3815–3818. http://dx.doi.org/10.1016/0016-7037(93)90159-T.

Usdowski, E., Michaelis, J., Böttcher, M.E., Hoefs, J., 1991. Factors for the oxygen isotope equilibrium fractionation between aqueous and gaseous CO_2, carbonic acid, bicarbonate, carbonate, and water (19 °C). Z. Phys. Chem. 170, 237–249.

Vargas-Hernández, J.M., Wijffels, S.E., Meyers, G., Belo do Couto, A., Holbrook, N.J., 2015. Decadal characterization of Indo-Pacific Ocean subsurface temperature modes in SODA reanalysis. J. Clim. 28:6113–6132. http://dx.doi.org/10.1175/JCLI-D-14-00700.1.

Venn, A., Tambutté, E., Holcomb, M., Allemand, D., Tambutté, S., 2011. Live tissue imaging shows reef corals elevate pH under their calcifying tissue relative to seawater. PLoS One 6, e20013. http://dx.doi.org/10.1371/journal.pone.0020013.

Wang, Z., Schauble, E.A., Eiler, J.M., 2004. Equilibrium thermodynamics of multiply substituted isotopologues of molecular gases. Geochim. Cosmochim. Acta 68: 4779–4797. http://dx.doi.org/10.1016/j.gca.2004.05.039.

Wang, Z., Gaetani, G., Liu, C., Cohen, A., 2013. Oxygen isotope fractionation between aragonite and seawater: developing a novel kinetic oxygen isotope fractionation model. Geochim. Cosmochim. Acta 117:232–251. http://dx.doi.org/10.1016/j.gca.2013.04.025.

Watkins, J.M., Hunt, J.D., 2015. A process-based model for non-equilibrium clumped isotope effects in carbonates. Earth Planet. Sci. Lett. 432:152–165. http://dx.doi.org/10.1016/j.epsl.2015.09.042.

Watkins, J.M., Nielsen, L.C., Ryerson, F.J., DePaolo, D.J., 2013. The influence of kinetics on the oxygen isotope composition of calcium carbonate. Earth Planet. Sci. Lett. 375: 349–360. http://dx.doi.org/10.1016/j.epsl.2013.05.054.

Watkins, J.M., Hunt, J.D., Ryerson, F.J., DePaolo, D.J., 2014. The influence of temperature, pH, and growth rate on the $\delta^{18}O$ composition of inorganically precipitated calcite. Earth Planet. Sci. Lett. 404:332–343. http://dx.doi.org/10.1016/j.epsl.2014.07.036.

Watson, E.B., 2004. A conceptual model for near-surface kinetic controls on the trace-element and stable isotope composition of abiogenic calcite crystals. Geochim. Cosmochim. Acta 68:1473–1488. http://dx.doi.org/10.1016/j.gca.2003.10.003.

Weiner, S., Addadi, L., 1991. Acidic macromolecules of mineralized tissues: the controllers of crystal formation. Trends Biochem. Sci. 16:252–256. http://dx.doi.org/10.1016/0968-0004(91)90098-G.

Xu, Z., Li, M., Patricola, C.M., Chang, P., 2013. Oceanic origin of southeast tropical Atlantic biases. Clim. Dyn. 43:2915–2930. http://dx.doi.org/10.1007/s00382-013-1901-y.

Zeebe, R.E., 2005. Stable boron isotope fractionation between dissolved $B(OH)_3$ and $B(OH)^{4-}$. Geochim. Cosmochim. Acta 69:2753–2766. http://dx.doi.org/10.1016/j.gca.2004.12.011.

Zeebe, R.E., Wolf-Gladrow, D., 2001. CO_2 in seawater: equilibrium, kinetics, isotopes. Equilibrium, Kinetics, Isotopes. Elsevier.

Zhang, R., 2007. Anticorrelated multidecadal variations between surface and subsurface tropical North Atlantic. Geophys. Res. Lett. 34, L12713. http://dx.doi.org/10.1029/2007GL030225.